Network-based systems pharmacology reveals heterogeneity in LCK and BCL2 signaling and therapeutic sensitivity of T-cell acute lymphoblastic leukemia

HHS Public Access

Author manuscript

Nat Cancer. Author manuscript; available in PMC 2021 September 01.

Published in final edited form as:

Nat Cancer. 2021 March ; 2(3): 284–299. doi:10.1038/s43018-020-00167-4.

Network-based systems pharmacology reveals heterogeneity in LCK and BCL2 signaling and therapeutic sensitivity of T-cell acute lymphoblastic leukemia

Yoshihiro Gocho[#1], **Jingjing Liu**[#2], **Jianzhong Hu**[#1], **Wentao Yang**[1], **Neekesh V. Dharia**[3,4], **Jingliao Zhang**[1], **Hao Shi**[5], **Guoqing Du**[1], **August John**[1], **Ting-Nien Lin**[1], **Jeremy Hunt**[1], **Xin Huang**[2], **Lauren Rowland**[1], **Lei Shi**[6], **Dylan Maxwell**[1], **Brandon Smart**[1], **Kristine Crews**[1], **Wenjian Yang**[1], **Kohei Hagiwara**[2], **Yingchi Zhang**[7], **Kathryn Roberts**[8], **Hong Wang**[9,10], **Elias Jabbour**[11], **Wendy Stock**[12], **Bartholomew Eisfelder**[12], **Elisabeth Paietta**[13], **Scott Newman**[2], **Giovanni Roti**[3,14], **Mark Litzow**[15], **Jinghui Zhang**[2], **Junmin Peng**[9,10], **Hongbo Chi**[5], **Stanley Pounds**[6], **Mary V. Relling**[1], **Hiroto Inaba**[16], **Xiaofan Zhu**[7], **Steven Kornblau**[11], **Ching-Hon Pui**[16], **Marina Konopleva**[11], **David Teachey**[17], **Charles G. Mullighan**[8], **Kimberly Stegmaier**[3,4], **William E. Evans**[1], **Jiyang Yu**[2,†], **Jun J Yang**[1,16,†]

[1]Department of Pharmaceutical Sciences, St. Jude Children's Research Hospital, Memphis, TN, USA

[2]Department of Computational Biology, St. Jude Children's Research Hospital, Memphis, TN, USA

[3]Department of Pediatric Oncology, Dana-Farber Cancer Institute and Boston Children's Hospital, Harvard Medical School, Boston, MA, USA

[4]The Broad Institute of MIT and Harvard, Cambridge, MA, USA

[5]Department of Immunology, St. Jude Children's Research Hospital, Memphis, TN, USA

[6]Department of Biostatistics, St. Jude Children's Research Hospital, Memphis, TN, USA

[7]State Key Laboratory of Experimental Hematology, National Clinical Research Center for Blood Diseases, Institute of Hematology & Blood Diseases Hospital, Chinese Academy of Medical Sciences & Peking Union Medical College, Tianjin, China

[8]Department of Pathology, St. Jude Children's Research Hospital, Memphis, TN, USA

[9]Departments of Structural Biology and Developmental Neurobiology, St. Jude Children's Research Hospital, Memphis, TN, USA

[†]Correspondence to: Jun J. Yang Ph.D., Member, Department of Pharmaceutical Sciences, Department of Oncology, jun.yang@stjude.org, Jiyang Yu Ph.D., Assistant Member, Department of Computational Biology, jiyang.yu@stjude.org, St. Jude Children's Research Hospital, 262 Danny Thomas Pl., Memphis, TN 38105.

Author Contributions

J.J.Y., J.Y., Y.G. and J.Hu designed the study and interpreted the results; Y.G., J.Hu, G.D., A.J., T-N.L., J.Hunt, L.R., D.M., B.S. performed the experiments; J.L., Wentao Y., Wenjian Y., H.S., X.H., K.H. S.P., L.S, and S.N. performed data analyses; N.V.D., Jingliao Z., L.S., K.C., Y.Z., K.R., H.W., E.J., W.S., B.E., E.P., G.R., M.L., Jinghui Z., J.P., H.C., S.P., M.V.R., H.I., X.Z., S.K., C.H.P., M.K., D.T., C.G.M., K.S. and W.E.E. contributed reagents, materials and analyses tools; J.J.Y., J.Y., Y.G., J.Hu and J.L. wrote the manuscript.

[10]Center for Proteomics and Metabolomics, St. Jude Children's Research Hospital, Memphis, TN, USA

[11]Department of Leukemia, The University of Texas MD Anderson Cancer Center, Houston, TX, USA

[12]University of Chicago Medical Center, Chicago, IL, USA

[13]Montefiore Medical Center, Bronx, NY, USA

[14]Department of Medicine and Surgery, University of Parma, Parma, Italy

[15]Division of Hematology, Mayo Clinic, Rochester, MN, USA

[16]Department of Oncology, St. Jude Children's Research Hospital, Memphis, TN, USA

[17]Department of Pediatrics, University of Pennsylvania, Philadelphia, Pennsylvania, USA

[#] These authors contributed equally to this work.

Abstract

T-cell acute lymphoblastic leukemia (T-ALL) is an aggressive hematological malignancy, and novel therapeutics are much needed. Profiling patient leukemia' drug sensitivities *ex vivo*, we discovered that 44.4% of childhood and 16.7% of adult T-ALL cases exquisitely respond to dasatinib. Applying network-based systems pharmacology analyses to examine signal circuitry, we identified preTCR-LCK activation as the driver of dasatinib sensitivity, and T-ALL-specific LCK dependency was confirmed in genome-wide CRISPR-Cas9 screens. Dasatinib-sensitive T-ALLs exhibited high BCL-XL and low BCL2 activity and venetoclax resistance. Discordant sensitivity of T-ALL to dasatinib and venetoclax is strongly correlated with T-cell differentiation, particularly with the dynamic shift in LCK vs. BCL2 activation. Finally, single-cell analysis identified leukemia heterogeneity in LCK and BCL2 signaling and T-cell maturation stage, consistent with dasatinib response. In conclusion, our results indicate that developmental arrest in T-ALL drives differential activation of preTCR-LCK and BCL2 signaling in this leukemia, providing unique opportunities for targeted therapy.

Introduction

Acute lymphoblastic leukemia (ALL) is a prototype of cancer that can be cured by pharmacotherapy alone[1,2]. In B-cell ALL (B-ALL), molecularly targeted agents are particularly effective in high-risk diseases, such as imatinib and dasatinib in ALL with the *BCR-ABL1* fusion or fusions involving other *ABL* class kinases[3–5]. ALL can also arise in a T-cell lineage, accounting for 12–20% of this leukemia[6]. T-ALL is characterized by a unique set of genomic features, including chromosomal rearrangements and enhancer mutations involving transcription factor genes such as *TAL1, TAL2, LMO1,* and *LMO2*[7,8]. T-ALL is associated with a more aggressive clinical presentation and historically inferior treatment outcome with cytotoxic chemotherapy, compared to B-ALL[9,10]. T-ALL becomes highly refractory to chemotherapy upon relapse, with a dismal prognosis[9,10]. Because there are presently no cellular or immunotherapies available in T-ALL[11], treatment options are very limited for this group of patients and novel therapeutic agents are much needed[6].

The current paradigm of cancer drug discovery often adopts a reverse genetics approach, i.e., developing small molecules that specifically target a genomic abnormality that is essential for cancer cell survival. For example, deregulated NOTCH signaling is an oncogenic driver in the majority of T-ALL and has been examined as a therapeutic target[12,13]. However, the clinical development of NOTCH-targeting agents has proven challenging, with the notable example of gamma-secretase inhibitor therapy[14,15]. Additionally, the mechanism of drug response is highly complex; therefore, efficacy of a drug that targets a single genomic aberration may be substantially influenced by a plethora of other tumor mutations or by unintended host effects. In fact, there are many clinical examples of non-response to targeted agents despite the presence of genomic lesions involving purported molecular targets[16,17]. In contrast, a forward genetics approach starts by determining the drug sensitivity phenotype of cancer cells and then examining the biological basis of drug response. For example, pharmacotyping of tumor samples can identify drug-sensitive patients to guide therapeutic decisions, agnostic of tumor genomics[18]. Subsequent genomic characterization of drug-sensitive and -resistant cases can then pinpoint the pharmacogenomic basis of inter-patient variation in response, which in turn would inform targeted therapy in future clinical trials. The utility of this approach has been illustrated in a number of recent pharmacotyping studies of both solid and liquid tumors[19–23], including ALL[24,25]. It should also be noted that biological processes operate through molecular networks, and singular focus on genomic aberration of individual genes overlook the “wiring” and “rewiring” of these networks that drive drug response. Therefore, network-based systems pharmacology analyses are particularly valuable in identifying signaling circuitry and non-genetic drivers of drug sensitivity in cancer, with notable success by us and others[26–28].

Originally developed as an ABL inhibitor, dasatinib is highly effective in chronic myelogenous leukemia and *BCR-ABL1* ALL[29]. Unlike imatinib and nilotinib, dasatinib has a broader spectrum of potential targets, including ABL and SRC-family kinases[30]. SRC-directed dasatinib inhibitory effects can be therapeutically beneficial in some settings, although at a concentration higher than that needed in *BCR-ABL1* leukemias[31–33]. This is also true in T-ALL, with a number of recent reports independently describing dasatinib sensitivity in a significant proportion of patients with this type of leukemia[33–35], with emerging evidence that points to LCK and preTCR sigaling as the putative therapeutic target. In fact, LCK activity is also required for proliferation and survival of T-ALL with ABL fusion gene, conferring dasatinib sensitivity[36]. However, the biological basis of inter-individual variability in dasatinib sensitivity in T-ALL is incompletely understood, with a particular paucity of systematic examination of regulators of dasatinib response beyond LCK and potential drivers of drug resistance. It is also unclear whether dasatinib sensitivity is related to T-ALL subtype, age, and treatment outcome with conventional chemotherapy.

Profiling leukemia drug response *ex vivo* for 352 cases of ALL, we identified 44.4% of childhood T-ALL with exquisite sensitivity to dasatinib. Our RNA-seq-based systems pharmacology analyses pointed to LCK-preTCR activation as the driver of dasatinib sensitivity in T-ALL, with orthogonal validation by phospho-proteomic profiling and genome-scale CRISPR-Cas9 screens. We also comprehensively evaluated the genomic and developmental basis of LCK activation in T-ALL, and explored mechanisms of dasatinib resistance by single cell analysis. Taken together, our results highlight opportunities for

molecularly targeted therapies in T-ALL, with a potential to impact the next generation of clinical trials for this type of leukemia.

Results

Ex vivo pharmacotyping revealed dasatinib response in T-ALL

To characterize the pattern of dasatinib response in ALL, we analyzed a cohort of 352 children and adults with ALL for whom drug sensitivity (measured as LC_{50}, the concentration at which 50% of leukemia cells were killed) was determined using a mesenchymal stromal cell co-culture assay *ex vivo*. This pharmacotyping cohort consisted of 239 adults (18 T-ALL and 221 B-ALL) and 113 children (27 T- and 86 B-ALL), representative of diverse molecular subtypes of ALL (Supplementary Table S1). Comprehensive genomic profiling was performed using RNA-seq, whole exome seq, and/or whole genome seq (Supplementary Table S2).

We observed a wide inter-patient variability in dasatinib sensitivity in ALL, with a bimodal distribution representing cases with low LC_{50} (mean at 6.04 nM [range 0.05 to 79.4]) or high LC_{50} (12,046.20 nM [101.65 to 20,000], Extended Data Fig. 1A). In B-ALL, cases with a *BCR-ABL1* fusion gene or fusions involving *ABL* class genes exhibited high sensitivity to dasatinib in both children and adults (Fig. 1A, Supplementary Table S3). The frequency of *BCR-ABL1* ALL was significantly higher in adults who consequently also showed a higher prevalence of dasatinib response than children with B-ALL (Extended Data Fig. 1B). Based on LC_{50} distribution in *BCR-ABL1* ALL (Extended Data Fig. 1C) we chose 80 nM as the cutoff to define dasatinib-sensitive vs -resistant ALL. In T-ALL, 15 (33.3%) cases were classified as dasatinib-sensitive, with a LC_{50} range largely indistinguishable from that of *BCR-ABL1* B-ALL (Fig. 1B and Extended Data Fig. 1D). Surprisingly, none of the dasatinib-sensitive T-ALLs harbored *ABL* class fusion genes. There was a trend for an over-representation of dasatinib-sensitive T-ALL in children compared to adults (44.4% and 16.7% of T-ALL, respectively, P=0.063 by Fisher's exact test, Fig. 1C). Testing three other ABL inhibitors in a subset of these primary T-ALL samples (N=18), we observed that dasatinib-sensitive cases were universally resistant to ABL-specific inhibitors imatinib and nilotinib, but responded to ponatinib which shares non-ABL targets with dasatinib (P=0.048 by Pearson correlation test, Fig. 1D–E and Extended Data Fig. 2A–B). In addition, we profiled eight human T-ALL cell lines for their sensitivity to dasatinib *in vitro*, of which three exhibited extreme response: ALL-SIL cell line with *NUP214-ABL* fusion, HSB-2 cell line with *TCR-LCK* fusion, and KOPT-K1 cell line with *TCR-LMO2* fusion (Extended Data Fig. 2C).

We randomly selected four dasatinib-sensitive T-ALL to confirm anti-leukemic efficacy *in vivo*, using patient-derived xenografts (PDXs, Fig. 2A–B). Given at 10 mg/kg twice daily, dasatinib significantly impeded leukemia growth in the recipient mice compared to those receiving vehicle control across the 4 cases (Fig. 2C), with prolonged leukemia-free survival ranging from 1.47 to 1.90-fold (Fig. 2D).

NetBID analyses identified preTCR-LCK activation as the driver of dasatinib sensitivity in T-ALL

To systematically examine biological factors underlying T-ALL response to dasatinib, we applied a data-driven network inference algorithm (NetBID)[37] to model signaling molecule activity from RNA-seq derived expression profiles (Fig. 3A and Supplementary Tables S4–5). First, we reverse-engineered, by using the SJARACNe algorithm[38], a T-ALL-specific interactome (T-ALLi) from the RNA-seq dataset of 261 unselected childhood T-ALL cases in the previously published TARGET ALL cohort[8]. The resultant T-ALL network consists of 27,179 genes and 1,068,228 interactions, representing 7,924 hub genes and their downstream targets. Overlaying T-ALLi to the RNA-seq dataset of 15 dasatinib-sensitive T-ALL and 30 resistant cases in the pharmacotyping cohort, we then inferred activity of each hub gene based on the expression of its targets weighed by the interaction strength of each hub-target pair. Compared to cases resistant to this drug, 193 and 268 hub genes showed a significantly higher or lower activity in dasatinib-sensitive T-ALL ($P< 10^{-5}$), respectively (Supplementary Table S6). In particular, we observed a remarkable enrichment of up-regulated genes in the pre-TCR signaling pathway (Fig. 3B, $P=9.6\times10^{-21}$), signified by *CD28, CD3E, CD3G, ICOS, CD40LG, LCK*, and *PTCRA* (Fig. 3C and Extended Data Fig. 3A). In parallel, we manually curated a list of 94 putative dasatinib targets, using DrugBank[39], DGIdb[40], and chemical proteomics-based TKI target profiling[41]. Of 13 targets identified in all three databases, SRC, LCK, FYN, and FGR showed a significantly higher activity in dasatinib-sensitive T-ALL, and LCK was the top hit with the most pronounced difference (Fig. 3D, Extended Data Fig. 3B–E, and Table S7). We also performed these analyses with pediatric cases alone to avoid confounding effects by age, and the results were highly concordant with those with all cases included (Extended Data Fig. 3F). Collectively, these results nominated LCK as the potential driver for dasatinib sensitivity in T-ALL.

To test this hypothesis, we selected seven dasatinib-sensitive and four resistant T-ALL cases to expand human leukemia cells in PDX for further functional experiments (Supplementary Table S2). Focusing on key components of the proximal preTCR signaling pathway immediately down-stream of LCK, we assessed the phosphorylation of LCK (Y394)[42], CD247 (Y142)[43], and ZAP70 (Y319)[44]. The level of tyrosine phosphorylation at baseline across these three proteins were markedly high in dasatinib-sensitive T-ALL cases and decreased dramatically upon dasatinib treatment in a dose-dependent fashion (Fig. 3E). By contrast, there was minimal phosphorylation of LCK, CD247, and ZAP70 in dasatinib-resistant T-ALL at baseline which also did not change by dasatinib. Similar results were observed in T-ALL cell line models HSB-2, KOPT-K1, and CEM (Extended Data Fig. 4A). To confirm dasatinib cytotoxicity is mediated through LCK inhibition, we examined the effects of LCK mutant T316M which is known to be resistant to dasatinib[45]. In KOPT-K1 cells, expression of the wildtype LCK or vector alone remained highly sensitive to dasatinib (LC_{50} of 0.0005 nM), whereas introduction of the T316M mutant led to a 25.8-fold increase in LC_{50}. In parallel, cells with wildtype LCK or the empty vector exhibited dose-dependent inhibition of LCK, compared to sustained LCK phosphorylation in cells expressing the T316M mutant, consistent with drug resistance (Extended Data Fig. 4B–E).

To globally explore dasatinib-mediated kinase inhibition, we selected three sensitive and two resistant T-ALL for phospho-proteomic profiling. In total, we identified 21,450 unique phosphosites across samples (Supplementary Table S8) and inferred activity of 172 human kinases based on the level of phosphorylation of their known substrates (Supplementary Table S9). In dasatinib-sensitive T-ALL, LCK, LYN, FYN, and INSR were significantly inhibited by dasatinib (Fig. 3F). In contrast, dasatinib-resistant T-ALL cells showed no significant changes in kinase activity before and after dasatinib treatment. Finally, because dasatinib can broadly inhibit SRC family kinases (including both SRC and LCK), we also tested T-ALL cases and cell lines with LCK inhibitors WH 4–023[46] and nintedanib[47]. Both compounds showed potent cytotoxicity in dasatinib-sensitive cases but not in dasatinib-resistant T-ALL ($P=7.8\times10^{-4}$ and 0.013 by Pearson correlation test for WH 4–023 and nintedanib, respectively, Fig. 3G and Extended Data Fig. 5). Together, these results indicate that the anti-leukemic activity of dasatinib in T-ALL is most likely mediated by LCK inhibition.

Genome-scale CRISPR-Cas9 screen validated LCK dependency in T-ALL

In parallel, we performed unbiased genome-scale CRISPR-Cas9 loss-of-function screening to identify genes essential to the growth and survival of T-ALL. Comparing the three T-ALL cell lines assayed (HSB-2, PF-382, and SUP-T1) to either all other cancer cell lines screened (N=686) or limited to hematologic malignancy cell lines (N=73), *LCK* emerged as the top selectively essential gene (Fig. 3H–I). *LCK* dependency varied amongst three T-ALL cell lines but was dramatically higher than cell lines from any other cancer types ($P=1.4\times10^{-34}$, Extended Data Fig. 4F). Interestingly, other preTCR pathway genes (e.g., *CD247*, *ZAP70*) also showed significant effects on T-ALL survival, consistent with the essential role of this signaling axis in T-ALL leukemia maintenance (Extended Data Fig. 4F). In contrast, deletion of SRC or other members of the SRC kinase family only minimally influenced T-ALL survival (Extended Data Fig. 4G).

Biomarker modeling predicted dasatinib sensitivity across T-ALL subtype

To build a robust biomarker model to predict dasatinib sensitivity in T-ALL, we used the pharmacotyping cohort of 15 sensitive and 30 resistant T-ALL cases, from which preTCR-LCK was identified, as the discovery dataset for training, and then collected an independent validation cohort of 5 dasatinib-sensitive and 8 resistant cases for testing. We first filtered the top 461 driver genes identified by NetBID analysis against preTCR pathway genes and dasatinib targets in the discovery cohort, resulting in a final panel of 30 markers, including *LCK* and *PTCRA* (Fig. 4A). Summing the weighed NetBID-inferred activity of these genes, we estimated a dasatinib biomarker score for each T-ALL case from their RNA-seq profile. Dasatinib-sensitive leukemias had significantly higher scores than those resistant to this drug in both the discovery cohort ($P=3.7\times10^{-7}$, Extended Data Fig. 6A), with replication in the validation set (P=0.023, Extended Data Fig. 6B, Supplementary Table S1). In the receiver operating characteristic curve analysis, dasatinib biomarker score achieved an area under the curve (AUC) value of 0.924 with a 95% confidence interval (CI) of 0.820—1.0 in the discovery cohort (Fig. 4B) and an AUC value of 0.85 with a CI of 0.624—1.0 in the validation cohort (Fig. 4C). At a cutoff value of 0.6, the dasatinib biomarker score achieved

a sensitivity and specificity of 0.933 0.767, and 1.0, 0.75, in the discovery and validation cohort, respectively.

Applying this dasatinib biomarker scoring algorithm to the RNA-seq dataset of 261 cases in the TARGET T-ALL cohort described above, we observed a wide variation in predicted dasatinib sensitivity across molecular subtypes (Fig. 4D and Extended Data Fig. 6C). T-ALL with overexpression of *TAL1*, *TAL2*, or *LMO1/2* genes exhibited the highest likelihood of dasatinib response whereas cases in the *LMO2/LYL1* subtype were the least sensitive to this drug ($P<2.0\times10^{-16}$ by ANOVA). Similarly, NetBID-predicted activities of LCK and PTCRA also vary by subtype, in a pattern consistent with the biomarker scores (Extended Data Fig. 6D–E). Dasatinib sensitivity biomarker score was negatively associated with treatment outcome of conventional cytotoxic chemotherapy (Fig. 4E): individuals predicted as dasatinib-sensitive (dasatinib biomarker score>0.6) showed a significantly worse event-free survival (EFS) than those with low predicted dasatinib sensitivity (dasatinib biomarker score≤0.6) (P=0.037, Cox regression test). The association of dasatinib sensitivity with EFS was particulary strong within the *LMO2-LYL1* T-ALL subtype (P=0.0016, Extended Data Fig. 6F). Further, T-ALL patients predicted to be dasatinib-sensitive also tend to have higher leukocyte count at diagnosis than those with low dasatinib biomarker scores ($P=3.3\times10^{-6}$) (Fig. 4F). These results pointed to potential benefits of adding dasatinib to the chemotherapy-based T-ALL treatment regimen.

T cell differentiation program and dasatinib sensitivity in T-ALL

From whole-genome and whole-exome seq, we did not observe a unifying somatic genomic abnormality that completely explained dasatinib sensitivity, although a number of features were notable (Fig. 5A and Supplementary Tables S10–12). *NOTCH1* mutations were detected in 93.3% of dasatinib responders compared to 50% in drug-resistant T-ALL (P=0.0069 by Fisher's exact test, detailed variants information in Fig. 5B), and a similar trend was seen with *FBXW7* mutation (33.3% vs 6.7%, P=0.032 by Fisher's exact test). Known to be associated with early T precursor ALL, mutations in the *DNM2* or *RUNX1* genes were only observed in cases resistant to dasatinib, suggesting LCK signaling may be dispensable in T-ALL with this immature immunophenotype.

Most notably, we identified *TCF7-SP1* fusion in one T-ALL case with exquisite sensitivity to dasatinib (LC_{50}=0.05 nM, Fig. 5A). Recently described as a novel subtype, *TCF7-SPI1* T-ALL is associated with a characteristic expression profile, including elevated expression of *PTCRA* and *LCK*[48]. We subsequently identified two additional T-ALL cases with the same *SPI1* fusion, and in both cases, we confirmed *ex vivo* sensitivity to dasatinib (LC_{50}=0.05 nM, Extended Data Fig. 7A). During normal T cell development, *PTCRA* expression is specifically turned on at the double negative 3a/3b (DN3a/3b) stage which in turn triggers a robust proliferative signal through LCK activation[49]. Therefore, we hypothesize that the differentiation arrest of *TCF7-SPI1* T-ALL at DN3 stage renders them vulnerable to LCK inhibition by dasatinib. In fact, applying the 30-gene biomarker model to expression profiles of murine T cell compartments at 19 differentiation stages[50], we noted that the predicted dasatinib sensitivity score rose sharply between DN2 and DN3 stages (Fig. 6A and Extended Data Fig. 8A), with a similar pattern observed for LCK and PTCRA activities (Extended

Data Fig. 8B). Conversely, we also compared the gene activity profile of each T-ALL case against these 19 stages during normal T cell development and quantified leukemia's similarity to different T cell compartments by clustering analysis. Dasatinib-resistant T-ALLs were most related to the early T-cell precursor (ETP) cells whereas dasatinib-sensitive cases were clustered closely to the DN3-DN4 T cells (Fig. 6A). We also explore NetBID analyses using human T cell expression profiles and again observed similar pattern of differentiation-related LCK and PTCRA activation (Extended Data Fig. 8C–E).

To test this experimentally, we isolated mouse Lineage^{-}Sca^{+}cKit^{+} cells (LSK cells) and transduced with either *TCF7-SPI1* fusion gene or empty vector as the control. Transduced LSK cells were then allowed to differentiate into various T cell subsets *in vitro* in the presence of OP9-DL1 cells. While the control LSK cells differentiated extensively into mature CD4/8 single positive T cells, *TCF7-SPI1*-expressing LSKs were unable to differentiate beyond the DN3 stage, which showed significantly higher levels of phosphorylation of LCK (Fig. 6C–D, Extended Data Fig. 7B). Similarly, we also observed variable dasatinib sensitivity across populations within mouse DN thymocytes: dasatinib induced robust growth inhibition of the DN3 cells and had little effects on DN1 and DN2 cells (Fig. 6E). Therefore, differentiation arrest at the DN3 stage represents a potential mechanism of LCK activation and dasatinib sensitivity, as exemplified in *SPI1*-rearranged T-ALL.

Dynamic shift of BCL2 and BCL-XL dependency during T-cell differentiation and its relation to T-ALL response to dasatinib and venetoclax

Among the top 461 driver genes for dasatinib sensitivity in T-ALL were BCL2 and BCL-XL. NetBID-inferred activity of BCL2 was significantly higher in dasatinib-resistant T-ALL than cases sensitive to dasatinib, whereas BCL-XL activity was positively associated with dasatinib response ($P=8.0\times10^{-7}$ and 1.3×10^{-7}, respectively, Fig. 7A–B). Similar to LCK, the activity of BCL2 and BCL-XL also shift dynamically across T-cell developmental stages. BCL2 is most up-regulated in ETP cells and its activity subdues as T cells become more mature, with the lowest value observed in the DN3-DN4 populations before it is activated again at the immature single positive (ISP) stage (Fig. 7C). By contrast, BCL-XL activity oscillates in a pattern that is opposite to BCL2, rising gradually from ETP to DN3 then followed by downregulation until T cells reach the ISP stage (Fig. 7C). Based on these observations, we postulated that dasatinib-sensitive T-ALL would be resistant to BCL2 antagonist venetoclax because of low BCL2 activity arising from developmental arrest at the DN3-DN4 stages. Testing venetoclax sensitivity *ex vivo* in the pharmacotyping T-ALL cohort (N=34), dasatinib-sensitive leukemia was indeed resistant to BCL2 inhibition-induced apoptosis (Fig. 7D). Venetoclax sensitivity *ex vivo* was associated with high BCL2 activity (Fig. 7E), whereas high BCL-XL activity was linked to resistance to venetoclax (Fig. 7F). Consistently, LCK activity was higher in venetoclax-resistant T-ALL than -sensitive cases (Extended Data Fig. 9A). To comprehensively identify biological basis for T-ALL sensitivity to venetoclax, we performed NetBID analyses and nominated 656 driver genes with P value < 0.001, with a highly significant enrichment of genes in the preTCR signaling pathway (Extended Data Fig. 9E). When we examined each of 7,441 genes included in the NetBID analysis for their effects on sensitivity to dasatinib vs. venetoclax,

there was a remarkable negative correlation (Fig. 7G), i.e., genes driving dasatinib sensitivity were almost always associated with venetoclax resistance. BCL2 and BCL-XL activity also varied significantly by T-ALL subtype (Fig. 7H–I).

Siimilarly, ETP cases in the TARGET T-ALL cohort showed the lowest activity score for LCK and BCL-XL. By contrast, ETPs had the highest BCL2 activity, consistent with previous report and their sensitivity to venetoclax[51] (Extended Data Fig. 9B–D).

Single-cell RNA-sequencing identified leukemia heterogeneity in preTCR and BCL2 signaling, T-cell maturation, and dasatinib response

To explore the biological basis of intra-tumor variability in dasatinib sensitivity, we performed single-cell RNA-sequencing (scRNA-seq) analysis of two dasatinib-sensitive T-ALL cases with detectable subclones as determined by TCRβ rearrangements (Supplementary Table. S13). For each case, we profiled leukemia cells with vs without exposure to dasatinib *in vitro*, and we postulate that cell that survived dasatinib would be drug resistant whereas vehicle-treated cells should remain naïve and drug sensitive (Supplementary Table S14). In SJ65, unsupervised clustering analysis of the scRNA-seq data identified three clusters, namely C1, C2, and C3, each of which consisted of both dasatinib-treated and naïve cells (Fig. 8A and Extended Data Fig. 9F). By computationally inferring the dasatinib biomarker score in each cell using NetBID, we observed distinct dasatinib biomarker scores, with C1, C2, and C3 predicted as the most sensitive, intermediate, and resistant to dasatinib (Fig. 8B). In fact, C3 primarily consisted of naïve leukemia cells sensitive to dasatinib (35.6% of cells), and this population was largely depleted upon dasatinib treatment. By contrast, cells that survived dasatinib were predominant in the drug-resistant cluster C1, and C2 included both sensitive and resistant populations (Fig. 8A and Extended Data Fig. 9F). NetBID-inferred activity of LCK was highest in the dasatinib-sensitive clusters C3 and C2 and decreased in drug resistant cluster C1, and the opposite trend was observed for BCL2 (Fig. 8C–D). In fact, at a single cell level, there was a striking inverse correlation of LCK and BCL2 activity ($R=-0.77$, $P<2.2\times10^{-16}$, (Fig. 8E), while BCL-XL and LCK activities exhibited a positive correlation ($R=0.49$, $P<2.2\times10^{-16}$, Extended Data Fig. 9G). Superimposing gene signatures of T-cell maturation stages, we observed a significant enrichment of ETP genes (e.g., *CD34*, *CD44*) in C1 and DN3/4 signature genes (e.g., *CD3D*, *CD3E*, *CD3G*, *ZAP70*, *CD28*, *LEF1*) in C3 (Fig. 8F and Supplementary Table S15). We repeated these analyses of single cell RNA-seq in the second T-ALL case and observed highly consistent results (Extended Data Fig. 9F–M). Taken together, these single cell profiling experiments indicated that the same biological regulators of dasatinib sensitivity identified from bulk RNAseq were also operative at the single cell level: DN3/4 stage with high LCK activity linked to sensitivity and ETP stage with high BCL2 activity linked to resistance, respectively. More importantly, our results identified subpopulations within individual T-ALL samples with heterogeneous signaling circuitry and drug response potential, which may explain the dasatinib resistance at relapse.

Integrating *ex vivo* drug profiling, multi-modality molecular profiling (whole transcriptomics, genomics, phospho-proteomics, and scRNA-seq) and functional genomic screening (Extended Data Fig. 10), we have identified hyperactivation of the preTCR-LCK

signaling as a highly effective therapeutic target in T-ALL. Our results suggest that T-ALL can retain signaling program activated in the maturation state where leukemia transformation occurs, giving rise to unique therapeutic vulnerability.

Discussion

Despite differences in the biology of B-ALL vs T-ALL, their current treatment regimens consist of nearly identical cytotoxic drugs. Therefore, exploring lineage-specific leukemogenesis processes is an exciting strategy to identify molecular targets for individualized ALL therapy. The association of preTCR-LCK activation with dasatinib sensitivity in T-ALL described herein is a particularly interesting example of lineage-dependent drug response. In early T-cell progenitors (double negative for CD4 and CD8), preTCRα serves as a molecular sensor for successful rearrangement of TCRβ. Only the successful assembly of the preTCR complex by the invariant preTCRα and productively-rearranged TCRβ would trigger a robust proliferative signal to expand these immature T cells, transmitted through LCK and a series of phosphorylation events. The proliferative signal set in motion by preTCR complex supports a pro-oncogenic effect in T-ALL leukemogenesis, as evidenced in different T-ALL mouse models[52,53]. The over-expression of *PTCRA* and concomitant LCK activation therefore could be a remnant of signaling events during leukemogenesis, but the strong anti-leukemic effects of preTCR signaling inhibition (by dasatinib) argue that it is also essential for leukemia maintenance. preTCR activation could also be the result of T-cell differentiation blockade when leukemia transformation occurs. For example, *SPI1*-rearranged T-ALL exhibits a highly characteristic immunophenotype indicative of a developmental arrest at the DN3 stage which is precisely when preTCRα expression is turned on and LCK is activated[54], likely explaining its dasatinib sensitivity.

Although dasatinib cytotoxicity is observed in both B- and T-ALL, the mechanisms of action are clearly lineage-specific, invoking inhibition of ABL and LCK (IC_{50} of 9 nM vs 17 nM, respectively[41]). Using a similar *ex vivo* drug sensitivity profiling approach, Bourquin et al. also described that ~30% T-ALL cases are sensitive to dasatinib and attributed the anti-leukemic effects to SRC inhibition[22]. By comparison, our systems pharmacology analyses clearly identified preTCR-LCK activation as the top distinguishing feature between dasatinib-sensitive vs -resistant T-ALL, corroborated by unbiased phospho-proteomic profiling as well as phospho-flow of LCK and its downstream targets in the preTCR pathway. Finally, our genome-scale CRISPR-Cas9 screen showed a consistent LCK dependency unique to T-ALL, whereas no other members of the SRC family affected T-ALL growth, providing further evidence that LCK inhibition is the driver for dasatinib sensitivity in this cancer. Beyond the preTCR pathway, our systems pharmacology analyses also identified a number of additional driver genes of dasatinib response in T-ALL, among which are BCL2 and BCL-XL. BCL2 and BCL-XL sequester pro-apoptotic molecules BAX or BAK and thus prevent commitment to cell death[55]. It has been known that normal T cells shift back and forth between BCL2 and BCL-XL as the primary antiapoptotic protein depending upon the differentiation stage[56]. In fact, this differential dependency is also retained in T-ALL, with ETP leukemia selectively exhibiting strong therapeutic response to BCL2 antagonist venetoclax[51]. This is in line with our observation that ETPs are almost

always dasatinib-resistant but sensitive to venetoclax. But importantly, the decrease of BCL2 with concomitant increase of BCL-XL overlaps with LCK activation around the DN3-DN4 stage, and the rise and fall of these drug targets creates a differentiation-dependent pattern of therapeutic vulnerability in T-ALL. Our single cell analysis further revealed substantial intra-leukemia heterogeneity in LCK and BCL2 activity and maturation stage. The population with high LCK activity resembled DN3-DN4 T cell whereas LCK^{low} population showed high BCL2 activity and transcriptional program similar to immature T cells. Therefore, the combination of dasatinib with venetoclax (or navitoclax) may be needed to maximally induce remission.

Our NetBID approach is distinct from traditional differential gene expression analysis in that we do not rely on comparing expression on an individual gene basis, instead the expression of multiple genes is used collectively in a network fashion to computationally predict the activity of the driver or "hub gene".[37] Comparing results from our gene activity-based analyses vs those from a differential gene expression approach, LCK and Pre-TCR pathway were not prominently identified by the latter (Extended Data Fig. 6G–H), suggesting that expression level alone is inadequate to reflect variation in gene activity.

It is noteworthy that *NOTCH1* mutation was significantly over-represented in dasatinib sensitive T-ALL compared to those resistant to this drug in our cohort (Fig. 5A). In normal T cell development, NOTCH signaling is highest during β-selection and coincides with preTCR signaling[49]. Therefore, it is plausible that NOTCH1 potentiates the proliferative signal arising from preTCR-LCK activation in dasatinib-sensitive T-ALL and as a result renders leukemia cells particularly reliant on LCK signaling for survival.

Dasatinib sensitivity also seemed to be more common in pediatric T-ALL cases compared to adults, although not significant with our small sample size. To further explore this, we analyzed an independent microarray-based T-ALL gene expression dataset[28], consisting of 37 adult and 191 pediatric patient samples. Applying NetBID analysis, we observed that dasatinib biomarker score in pediatric cases is significantly higher than in adults in this cohort (Extended Data Fig. 6I–J, P=0.0012). Interestingly, pediatric cases have a higher prevalence of subtypes predicted to be dasatinib-sensitive (e.g., TAL1 and TAL2, Figure 4D), whereas dasatinib-resistant subtypes (e.g., HOXA and LMO2/LY1) are enriched in adults (Extended Data Fig. 6I–J). In a multivariate regression analysis, the association of age with dasatinib biomarker score was no longer significant after adjusting for subtype (P=0.3). Therefore, the differential distribution of T-ALL subtype between children and adults likely contributes to the age pattern in leukemia sensitivity to dasatinib, although this needs to be further validated with a larger sample size and mechanistically.

A dasatinib-based therapy in T-ALL is clinically attractive because this drug has already been approved for pediatric and adult ALL (with *BCR-ABL1* fusion) with a tolerable toxicity profile[3]. Currently for children with Ph+ ALL, dasatinib is given orally at 60–80mg/m^2/dose b.i.d[3,57], with median Cmax values between ~100 and 200 ng/ml[58–60]. These values translate to a plasma drug concentration of 200–400 nM, which is significantly higher than mean LC_{50} in dasatinib-sensitive T-ALL (6.04 nM) based on *ex vivo* drug sensitivity profiling. Therefore, it is reasonable to expect systemic drug exposure achievable with

current dasatinib dosing and dosing schedule is sufficient for LCK inhibition in T-ALL *in vivo*. Because ponatinib is also known to inhibit LCK (IC_{50}=55 nM)[41] and showed cytotoxic effects *ex vivo* in a subset of our pharmacotyping T-ALL cases (Fig. 1D), it would be of interest to evaluate this agent in future studies and compare it against dasatinib.

In conclusion, our systems pharmacology study identified biological factors related to inter-patient variability in response to targeted therapeutics in T-ALL, namely dasatinib and venetoclax. The development of biomarker-guided clinical trial to test these agents (or combination) is needed to translate this laboratory discovery into improved clinical outcome of T-ALL in the near future.

Methods

Patients and samples

The ALL cases included for pharmacotyping consisted of 129 pediatric cases from St. Jude Children's Research Hospital (NCT03117751) and the Children's Oncology Group; and 243 adults from MD Anderson Cancer Center, University of Chicago, ECOG E1910 clinical trial (NCT02003222), and the Alliance A041501 trial (NCT03150693). The main T-ALL cohorts consist of the pharmacotyping discovery set of 45 cases and a validation set of 13 cases, all of which were subjected to RNA-seq and used for the systems pharmacology analysis (i.e., NetBID). Details of molecular profiling assays and functional experiments performed for each ALL sample are provided in Supplemental Tables S2 and S3.

Leukemia blasts were obtained from either bone marrow or peripheral blood after Ficoll gradient centrifugation. Samples were subjected to further enrichment by magnetic-activated cell sorting if blast percent was below 85% (CD19 for B-ALL and CD7 for T-ALL, respectively). Leukemia cells were subjected to drug sensitivity profiling *ex vivo* for a panel of anti-leukemic drugs (Extended Data Fig. 1E). Bone marrow or blood was collected during remission and used as germline samples.

This study was approved by the respective institutional review boards at St. Jude Chhildren's Research Hospital, MD Anderson Cancer Center, University of Chicago, Children's Oncology Group, the ECOG-ACRIN Cancer Research Group, the Alliance for Clinical Trials in Oncology, and informed consent was obtained from parents, guardians, and/or patients, as appropriate.

Statistics and reproducibility

Sample size was not statistically predetermined for systems pharmacology analyses and maximal number of cases were included based on sample and data availability, without other filtering. Mice were randomly assigned to experimental groups to avoid bias and only female mice were used to ensure engraftment efficiency. All statistical testes were two-sided and were chosen as appropriate to data distribution; the threshold for statistical significance was defined as $P<0.05$ or lower with consideration of multiple testing. In the treatment outcome analysis, event free survival was considered as a time-to-event variable, and its relation to the t-SNE-based clusters was assessed by using the Cox proportional hazard regression model adjusting for T-ALL molecular subtypes and genetic ancestry. Events included

relapse, second cancers, death in remission, etc. We did not exclude any data and replicate experiments were stated in the legends of each figure. Details of preproducibility are included in the Reporting Summary.

Genomic profiling

For total RNA-seq, library was constructed from leukemia RNA using Illumina TrueSeq stranded mRNA library prep kit and sequenced using the HiSeq or NovaSeq platforms (2 × 101- bp pair-end reads). On average, we achieved at least 20x coverage for more than 30% of the transcriptome. RNA-seq analyses were performed using our previously established procedures[61]. Gene expression was quantified as Fragments Per Kilobase of transcript per Million mapped reads (FPKM) using RSEM v1.2.28PP with the hg GRCh38 and annotation file (Gencode v30). CICERO (v0.30.) was used to detect fusions[62] and the reported fusion contigs were remapped by BLAT to check reliability of mapping quality, breakpoints were manually reviewed from the aligned reads.

For whole exome seq, libraries were prepared using the Nextera rapid capture expanded exome kit and subjected to pair-end sequencing (101 bp read length) on the HiSeq or NovaSeq platforms. On average, we achieved 20x coverage for a median of 71% exome. For whole genome seq, libraries were constructed using Kapa Hyperprep kit (Roche) and sequenced for 2 × 151 bp pair-end reads. Whole exome seq and whole genome seq analyses were performed following procedures established previously[61,63]. Reads were aligned to the hg GRCh37 by BWA (version 0.7.12). Picard (version 1.129) was used for marking PCR duplication, the reads were realigned around potential indel regions by GATK IndelRealigner module (version 3.5). The MuTect2 module (version 4.1.0.00) from GATK was used to identify single nucleotide variants and indels, with annotation using ANNOVAR (version 20191024). Tumor copy-number variations and structural variations were detected using CONSERTING (version 1.0)[64] and CREST (version 1.0)[65].

For cases with leukemia RNA-seq data only, we used the GATK pipeline to infer single nucleotide variants and indels from RNA-Seq with the HaplotypeCaller module (version 4.0.10.0). We only included variants called in genes in which mutations were detected in other cases by whole genome or whole exome seq.

Whenever appropriate, we performed SNP microarray profiling to determine copy number status, using either Illumina Infinium Omni2.5 Exome-8 and/or Affymetrix Genome-Wide Human SNP Array 6.0. Our analytical pipeline for copy number was described previously[66].

The previously published RNA-seq data from the TARGET T-ALL cohort[8] was used for network building and biomarker analyses as described below. T-ALL subtype was defined using expression profile-based clustering analysis, following procedures reported previously[8].

Ex vivo leukemia drug sensitivity assay

Drug response of primary human ALL cells was evaluated using a co-culture system and flow cytometry assays. hTERT-immortalized mesenchymal stem cells[67] (provided by Dr. Dario Campana from National University of Singapore) were first seeded in a 96-well plate

format at a density of 10,000 cells per well in 100ul of complete medium (RPMI-1640, L-glutamine, 10% fetal bovine serum and 1μM Hydrocortisone). After 24 hours, leukemia cells were added at 160,000 cells per well to the stromal cell layer in 80 μl AIM-V medium along with 20 μl of drug solution prepared in the same medium. Duplicates were included for each of the six drug concentrations (10000, 1000, 100, 10, 1, 0.1 nM for dasatinib/ponatinib/nilotinib; 2500, 250, 25, 2.5, 0.25, 0.025 nM for imatinib; 100, 10, 1, 0.1, 0.01, 0.001 nM for venetoclax). After 96 h incubation at 37°C with 5% $CORR_2RR$, cells were harvested and stained with CD19 or CD7 to identify leukemia blasts (for B- and T-ALL, respectively). The total number of live leukemia cells were evaluated by using flow cytometry after Annexin V and DAPI staining. Drug-induced death was estimated by comparing to leukemia cells treated with the vehicle alone. The drug concentration that killed 50% of the leukemia cells ($LCRR_{50}RR$ value) was determined with a dose-response model. Quality control was performed to remove cases with low viability (less than 1000 viable blast cells in each well in the absence of drugs on day 4). For cases with which even the lowest dasatinib concentration kills more than 50% of leukemia cells, $LCRR_{50}RR$ was assigned as 0.05 nM. Conversely, for cases with >50% viability even at the highest drug concentration, $LCRR_{50}RR$ was assigned as 20000 nM.

Construction of T-ALL interactome via SJARACNe

To reverse engineer a T-ALL specific interactome (TALLi), we applied SJARACNe (version 0.2.0)[38] to the TARGET T-ALL RNA-seq dataset[8] with expression profile of 27,218 unique genes from 261 patients, after removing 5,820 genes with low or invariable expression and three outlier cases. Based on Gene Ontology classification, we compiled a list of transcription factor genes and signaling molecule genes (N=2,002 and 9,626, respectively). Transcription factor network and signaling molecule network were generated separately using SJARACNe, with drivers (hubs) linked to their targets through interactions (edges) based on gene-gene relationship derived from their expression pattern. The transcription factor network contained 27,063 nodes and 484,160 edges; signaling network included 26,927 nodes and 584,068 edges. After combining these two networks, the final TALLi consisted of 35,102 nodes and 1,068,228 edges, among which, there were 7,924 unique hub genes (1,653 transcriptional factors and 6,271 signaling molecules).

Genome-scale CRISPR-Cas9 screen and analysis

We first engineered T-ALL cell lines HSB-2, PF-382, and SUP-T1 to stably express Cas9, following procedures described previously[68]. Briefly, 4×10^6 T-ALL cells were virally transduced with 4000 ng pCMV-VSV-G (Addgene #8454), 2000 ng pCMVdeltaR8.91, and 8000 ng pLX311-Cas9 (Addgene #118018) or pXPR_011_EGFP (Addgene #59702). Cells were selected with 8 ug/ml blasticidin (for pLX311-Cas9 expressing cells) (Sigma-Aldrich, St. Louis, MO, USA, # SBR00022) or 1 ug/ml puromycin (Invitrogen, San Diego, CA, USA #ANT-PR-1) (for pXPR_011 expressing cells). Optimal infection conditions were determined for each T-ALL cell lines in order to retain a Cas9 activity greater than 50% (i.e., the fraction of EGFP positive and EGFP negative as measured by flow cytometry).

Cas9-expressing T-ALL cell lines HSB-2, PF-382, and SUP-T1 were then used for the genome-scale CRISPR-Cas9 screen, as part of the Cancer Dependency Map project at the

Broad Institute[69]. This screen was conducted as previously described[68] and data analyses (e.g., dependency score) were performed following procedures describe by Dempster *et al.*[69]. Briefly, cancer cell lines with constitutive expression of Cas9 were infected in replicate (n=3) at low multiplicity of infection (MOI<1) with the Avana sgRNA library containing >70,000 unique sgRNAs with an average of 4 guides per gene and approximately 1,000 nontargeting control guides. Cells were selected in puromycin and blasticidin for 7 days and then passaged for 21 days after infection. Genomic DNA was purified and guide RNAs were PCR amplified and sequenced with standard Illumina protocols. The resulting read counts for each sgRNA per cell line replicate were processed as described previously[69] to generate gene effect scores for each gene in each cancer cell line. To determine the genetic dependencies that were enriched in T-ALL cell lines, we utilized linear-model analyses from the limma R package (version 3.44.3) to perform a two-tailed t-test for the difference in distribution of gene effect (dependency) scores in T-ALL cell lines compared to other cell lines screened. Statistical significance was calculated as a q-value derived from the p-value corrected for multiple hypothesis testing using the Benjamini & Hochberg method[70].

NetBID analysis to identify drivers of dasatinib sensitivity in T-ALL patients

A total of 45 T-ALL were included in the NetBID analysis(version 0.1.2) to identify drivers of dasatinib sensitivity. Dasatinib $LCRR_{50}$RR in ALL largely followed a bi-modal distribution, and we defined sensitive and resistant as $LCRR_{50}$RR less or greater than 80nM, respectively, with dasatinib $LCRR_{50}$RR of *BCR-ABL1* B-ALL as the reference (Extended Data Fig. 1C). Therefore, subsequent analysis was performed comparing 15 sensitive vs 30 resistant T-ALL cases.

Expression profile was extracted from RNA-seq data for 18,294 genes and used for NetBID analysis. Then ***cal.Activity*** function (method= 'weightedmean') in NetBID was employed to infer the activities of driver genes for each patient from their gene expression profiles and the TALLi. The weighted mean activity of a hub (driver) gene *i* in sample s was defined by the following equation:

$$HUBsi = \frac{\sum_{j=1}^{n} SIGNij * MIij * EXPsj}{n}.$$

The gene expression matrix was Z-normalized in each sample and *EXPsj* is the expression value of gene *j* in sample s. *MIij* is the mutual information between driver gene *i* and its target gene *j* and *SIGNij* is the sign of spearman correlation between gene *i* and its target gene *j*. The total number of targets for driver *i* is denoted by *n*.

To identify drivers of dasatinib sensitivity in T-ALL, differential activity (dasatinib sensitive cases vs. resistant cases) was calculated by NetBID function ***getDE.BID.2G***. We also performed pathway analysis to identify the enrichment of drivers in specific biological processes by querying the KEGG pathway database[71] and evaluated the statistical significance of the enrichment using the Fisher's exact test. In addition, we curated DrugBank[39], DGIdb[40], and chemical proteomics-based TKI target profiling[41] to compile a

list of putative dasatinib targets whose enrichment in the 461 drivers was again evaluated by using the Fisher's exact test.

We also performed traditional differential gene expression analysis using the RNA-seq dataset described above. The expression of each gene was compared between dasatinib-sensitive vs. -resistant T-ALL in the discovery cohort, using the ***getDE.limma.2G*** function in the NetBID package.

NetBID analysis to identify drivers of venetoclax sensitivity in T-ALL patients

We profiled venetoclax sensitivity *ex vivo* for 34 of 45 T-ALL patient samples within the dasatinib pharmacotyping cohort. Applying NetBID, we evaluated the association of gene activity with venetoclax $LCRR_{50}RR$ using the non-parametric Spearman correlation. Venetoclax $LCR_{50}RR$ did not follow a bimodal distribution and thus were treated as a continuous variable in this analysis.

Dasatinib biomarker panel and sensitivity score

We derived a 30-gene biomarker panel by filtering the 461 NetBID-predicted drivers against the known dasatinib target genes and genes in the preTCR pathway. To estimate biomarker-based dasatinib sensitivity score for a given patient, we first standardized the RNA-seq profile ($logRR_2RR$-transformed FPKM) by z-transformation to make it comparable across samples, and then calculated the activities of 30 drivers individually using our T-ALLi and the ***cal.Activity*** function (method= 'weightedmean') in NetBID. For a given T-ALL case, we took a weighted (+1 for positive drivers and −1 for negative drivers) mean of activities of all 30 drivers as the dasatinib sensitivity score.

$$Ss = \frac{\sum_{i=1}^{30} Zi * Dsi}{30}.$$

Ss is the summarized dasatinib sensitivity score of sample *s*. Zi is the *z* score of driver *i* between sensitive and resistant samples and *Dsi* is the driver *i* activity in sample *s*.

Dasatinib sensitivity score was estimated for 261 cases in the TARGET T-ALL dataset[8] and 45 cases samples in the pharmacotyping T-ALL cohort. We also applied this biomarker model to the gene expression dataset of 19 mouse T cell populations[50], to infer dasatinib sensitivity across development stages. Finally, we estimated biomarker score in microarray-based T-ALL gene expression data[72], after removing control probes, probes targeting multiple genes, and then used ***IQR.filter*** function in NetBID (thre=0.2) to select variable genes for inferring gene activity and biomarker score as described above.

T-ALL differentiation staging

Gene activities were inferred using NetBID from the expression dataset of mouse T cell populations[50], as described above, and then mapped to human genes using BioMart[73]. Genes with species-specific activities were excluded, and then T-ALL and normal T cell gene activity profiles were pooled with the final dataset of 465 genes with coefficient of

variation >0.5. Applying t-SNE to this dataset, we performed clustering analysis of T-ALL and normal T cells. Cluster groups were determined using the *k*-means method. We also performed similar analyses using gene expression profiles of human T-cell populations[74].

Phospho-proteomics and data analyses

Human T-ALL cells from 3 dasatinib-sensitive and 2 resistant cases were selected for proteomic studies. A total of 20 million cells were incubated with 10 nM dasatinib or vehicle in 10cm^2 petri-dishes and incubated for one hours. Cells were then harvested and washed rapidly using cold PBS, and cell pellets were placed in liquid nitrogen for 30 min and stored at −80°C. Each T-ALL case was tested as a singlet. Proteomic assays were performed following previously published procedures[75]. Briefly, cell pellets were lysed and digested into peptides, which were then labeled with tandem-mass-tag reagents and enriched for phosphopeptide using TiORR$_2$RR. Reverse-phase LC and tandem mass spectrometry were performed to quantify phospho-peptides. After curation using the JUMP software suite and applying a false discovery rate cutoff of 1%, our final dataset consisted of 27,757 phosphopeptides. For phosphosites mapped to multiple peptide fragments, we selected the phosphopeptide with the most significant difference in dasatinib-treated vs. untreated T-ALL samples, which resulted in 21,450 unique phosphosites for subsequent analyses.

We infer kinase activity based on the substrate phosphorylation levels, using the PhosphoSitePlus database[76] to define 10,594 kinase-substrate pairs (359 human kinases). Of these, we detected phosphorylation events in our T-ALL phospho-proteome dataset, related to 1,223 pairs linked to 172 kinases. We estimated the activity of each kinase by using the following equation:

$$Ki = \frac{\sum_{j=1}^{n} log2(pij)}{n}$$

The intensity of each phosphosite was logRR$_2$RR-transformed and Z-normalized in each sample. P*ij* is the abundance of phosphosite *j* which is phosphorylated by the Kinase *i*. The kinase *i* activity can be defined by its ability to phosphorylate substrate sites, which was estimated by the mean intensity of the kinase substrate phosphosites.

We used NetBID to compare inferred kinase activity between dasatinib-treated and baseline samples in the dasatinib- sensitive or -resistant group separately, using linear modeling.

Phospho-flow of LCK signaling molecules

Human leukemia cells were collected and incubated overnight, before exposed to dasatinib for one hour. Cells were then harvested and resuspended in cold PBS. Pre-warmed (37°C) Lyse/Fix buffer (BD Phosflow™, #558049) was added, and cells were incubated at 37°C for 10 minutes, and fixed cells were premetallized with pre-chilled Perm Buffer III (BD Phosflow™, #558050) for 30 minutes on ice.

Fixed and permeabilized cells were stained with CD3 (BD Pharmingen™, #558117) and phospho-antibodies targeting SRC-Y418/LCK-Y394 (BD Phosflow™, #560095/560096),

CD247-Y142 (BD Phosflow™, #558448), and ZAP70-Y319 (BD Phosflow™, #557881) (all antibodies were diluted at 1:50) and then run on flow-cytometer (MACSQuant® × Flow Cytometer, Miltenyi Biotec). All phospho-flow data were analyzed by FlowJo (version 10.5.3)™.

Patient derived xenograft (PDX) and *in vivo* evaluation of dasatinib therapy

PDXs were developed for 11 T-ALL cases in this cohort, using the NOD.Cg-*Prkdc*^{scid} *Il2rg*^{tm1Wjl}/SzJ (NSG) mice. Cases were selected solely based on whether sufficient material was available for xenografting. All animal studies were approved by the Institutional Animal Care and Use Committee of St. Jude Children's Research Hospital. For each case, primary human T-ALL cells were injected into female NSG mice between 8–12 weeks of age through tail vein (2 million cells/mouse). All NSG mice were housed in sterilized condition at 20–23°C and 40–60% humidity, a 12 light/12 dark cycle was applied. Health status of all injected mice were monitored daily. Starting from two weeks after injection, peripheral blood was sampled to monitor the level of human leukemia by flow cytometry (cells were stained with TER119 (BD Pharmingen, #560512), mCD45 (BD Pharmingen, #557659), CD45 (BD Pharmingen, #555482), CD7 (BD Pharmingen, #555361), all diluted at 1:100 ratio; humanCD45 and humanCD7 double positive percentage was determined using BD FACS Aria IIIu machine & BD FACS LSR II machine (BD FACS Diva Software V8.0.1)) every other week. Mice were euthanized when leukemia reached 80% in blood or they became moribund, and human leukemia cells were harvested from spleen and bone marrow and enriched using immunomagnetic isolation kit (Stemcell, #19849).

Dasatinib efficacy was evaluated *in vivo* in 4 T-ALL PDX models. Dasatinib (LC Laboratories, #D-3307) was dissolved in citric acid (Jena Bioscience, #CSS-508) and was administrated at 10 mg/kg twice daily through oral gavage. Leukemia burden was monitored in blood with the same procedure and endpoints as above.

Rescue experiment by overexpression of T316M mutant LCK

LCK overexpression construct was cloned from Cl20c-IRES-GFP vector with wildtype human LCK cDNA insertion (cl20c-LCK-IRES-GFP). Primers for T316M mutagenesis was designed by QuikChange webtool (https://www.chem.agilent.com/store/primerDesignProgram.jsp): forward primer 5'ggagcccatctacatcatcatggaatacatggagaatgggag3', and reverse primer 5'ctcccattctccatgtattccatgatgatgtagatgggctcc3. Mutagenesis was performed using Agilent QuikChange Lightning Site-Directed Mutagenesis Kit (Agilent, #210518). Lenti-virus was packaged and stored in −80°C prior to use.

To measure dasatinib/ponatinib/imatinib sensitivity of KOPT-K1 expressing mutant or wildtype LCK (or vector control), a flow-based assay was performed as described in the *ex vivo* leukemia drug sensitivity assay section. After intracellular staining with LCK-Y394-Alexa647 (BD Phosflow™, #560096, 1:50 dilution), phosphorylation of KOPT-K1 cells treated with dasatinib for one hour was examined by phospho-flow, as described above.

Functional studies of *SPI1* fusion in T-ALL

To overexpress *TCF7-SPI1* fusion gene, we utilized a MSCV-IRES-mCherry vector (originally from MSCV-IRES-GFP, Addgene, #20672) and inserted cDNA for the fusion gene. To isolate hematopoietic progenitor/stem cells, mouse (C57BL/6) bone marrow cells were harvested and resuspended in MACS buffer (2mM EDTA/0.5% BSA/PBS). Cells were then stained with CD117 MicroBeads (Miltenyi Biotec, #130-091-224) and positively sorted with magnetic columns (LS column, Miltenyi Biotec, #130–042-401) and separator (QuadroMACS™ Separator, Miltenyi Biotec, #130-091-051) to enrich CD117 positive cells. After overnight incubation, CD117 enriched cells were stained with antibodies against CD117 (BD Pharmingen, #560557) and Sca-1 (BD Pharmingen, #560654) and sorted for double positive population (LSK cells). LSK cells were loaded onto virus-coated plate and centrifuged at 423 *g* for 10 minutes at room temperature, and cells were sorted for mCherry positive cells 2 days later.

To evaluate LSK cell differentiation *in vitro*, we adopted the OP9-DL1 co-culture assay, following procedures established previously[77].

To determine dasatinib sensitivity in each DN stage, mouse thymocytes were isolated from C57BL/6 thymus and DN cells were enriched by removing CD4/8 positive cells. DN cells were then allowed to grow *in vitro* for 2 days on supportive OP9-DL1 cells with and/or without dasatinib. Cells were stained with CD4-PE-Cy7 (BD Pharmingen, #552775), CD8-APC (BD Pharmingen, #561093), TER119-BV421 (BD Horizon™, #563998), CD4-PacBlue (BD Pharmingen, #558107); CD8-BV421 (BD Pharmingen, #562428), CD45-BV711 (BD Horizon™, #563685), CD44-APC (BD Pharmingen™, #559250), and/or CD25-PE-Cy7 (BD Pharmingen™, #552880); all antibodies were diluted at 1:100 ratio; and viable cell counts in all DN populations were measured by flow-cytometry and compared between dasatinib treated and untreated groups.

To validate the association of *SPI1* fusion with dasatinib sensitivity, we identified two additional human T-ALL cases with *TCF7-SPI1* fusion at St. Jude and the Institute of Hematology and Blood Diseases Hospital, Chinese Academy of Medical Sciences.

Single cell RNA-seq

scRNA-seq was performed using PDX cells from two T-ALL patient samples (SJ65 and SJ53). Following RBC lysis (Qiagen, #158904), human leukemia cells were enriched by EasySep™ Mouse/Human Chimera Isolation Kit (StemCell #19849) and then resuspended in culture media (RPMI1640 Gibco #11875–093 with 20% FBS GE life sciences #SH30071.03). 10nM dasatinib or vehicle was added to culture, followed by incubation at 37C with 5% $CORR_2R$R for four days. Cells were then harvested and subjected to lysis, library construction, and sequencing.

Alignment, barcode assignment and unique molecular identifier counting—

The Cell Ranger 3.1.0 Single-Cell software suite (10X Genomics) was implemented to process the raw sequencing data from the Illumina HiSeq run. This pipeline performed demultiplexing, alignment (hg GRCh38) and barcode processing to generate gene–cell matrices used for downstream analysis. Specifically, data from PDX samples with vehicle or

dasatinib treatment were combined into one dataset for consistent filtering. SJ65 and SJ53 corresponding to two T-ALL primary samples were analyzed separately. Cells with low or high UMI counts were filtered, as well as those with high mitochondria gene reads (>12.6%). A small fraction of outlier cells was further removed because of their low transcriptome diversity. For SJ65, a total of 13,992 cells were captured, with an average of 5,455 mRNA molecules. For SJ53, a total of 12,292 cells were captured, with an average of 7,556 mRNA molecules. We normalized the expression level of each gene to 100,000 UMIs per cell and log-transformed them by adding 1 to the expression matrix.

Clustering analysis and data visualization—For the clustering analysis, we modified the Single-Cell Consensus Clustering (SC3) algorithm (version 3.12)[78] as the following. We first used mutual information as a distance metric to reconstruct cell-cell similarity matrix and then performed multidimensional scaling analysis (MDS). To obtain robust clustering results, we perform consensus k-means clustering by using the first 16–19 dimensions. By testing various k values, we converged into 3 clusters for both cases. For visualization of clustering results, we used t-distributed stochastic neighbor embedding (t-SNE) with the first 19 MDS dimensions as the input. Gene activity and dasatinib biomarker score were calculated using NetBID as describe above. To obtain ETP and DN3/4 thymocytes signatures, gene expression (preT.ETP.Th and preT.DN3–4.Th from GEO datasets: GSE15907) was compared between each other ($LogRR_2RRFC > 0.5$ or $LogRR_2RRFC < -0.5$) using limma R package v3.44.3. The expression of each gene in the signature was averaged across cells within each cluster and then scaled and color-coded based on z-score.

Cell line and chemicals

hTERT MSCs (Mesenchymal Stem Cell) were maintained in RPMI1640 (Gibco, #11875093) with 2mM L-Glutamine (Gibco, # 25030081), 10% FBS (GE life sciences, #SH30071.03) and 1μM hydrocortisone (Sigma-Aldrich, #H0888); T-ALL cell lines Jurkat, CEM, RPMI-8402, MOLT-4, KOPT-K1 and DND-41 were maintained in RPMI1640 with 10% FBS; other T-ALL cell lines HSB-2 and ALL-SIL were maintained in RPMI1640 with 20% FBS. All cells were incubated at 37°C with 5% CO_2.

Drugs were purchased from Selleckchem: dasatinib (#S1021), ponatinib (#S1490), nilotinib (#S1033), WH 4–023 (#S7565), nintedanib (#S1010) and venetoclax (#S8048).

Cell line drug sensitivity profiling using the MTT assay

Drug sensitivity was determined for ALL cell lines using MTT assay, following procedures described previously[79]

Data Availability Statement

Details of data access are provided on the permalink page on St. Jude Cloud (https://pecan.stjude.cloud/permalink/PGx-TALL). Briefly, genomic data are available at St. Jude Cloud (SJC-PB-1022), NCBI GEO (GSE158457), and EGA (EGAS00001004700). Genome-scale CRISPR-Cas9 screen result can be obtained at the DepMap Portal (https://depmap.org/portal/achilles) with raw data available at FigShare (https://figshare.com/articles/dataset/DepMap_19Q4_Public/11384241/3).

TARGET T-ALL dataset is available in dbGAP (phs000218 and phs000464), and the microarray-based T-ALL expression profile is at NCBI GEO (GSE32215). Drug Bank database is at go.drugbank.com, KEGG pathway database is at genome.jp/kegg/pathway.html. The data that support the findings of this study are available from the corresponding authors upon request.

Code Availability Statement

Codes for NetBID analysis and dasatinib biomarker score calculation are available at GitHub (https://github.com/jyyulab/dasatinib-TALL).

Extended Data

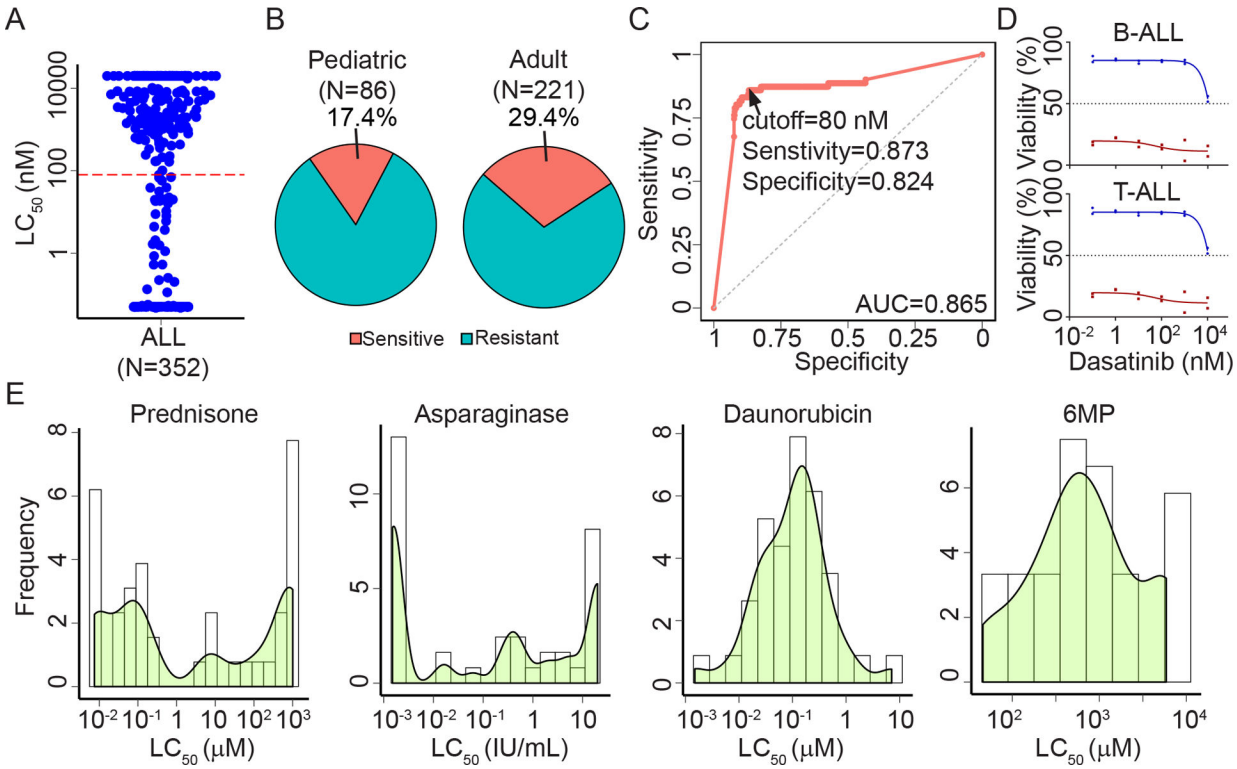

Extended Data Fig. 1. ALL sensitivity to dasatinib and cytotoxic drugs.

A. Dasatinib LC_{50} distribution of all 352 ALL patient samples (including 307 B-ALL and 45 T-ALL samples). **B.** Of 86 pediatric B-ALL samples, 17.4% were sensitive to dasatinib, whereas 29.4% of 221 adult B-ALL samples were dasatinib-sensitive. **C.** Dasatinib LC_{50} reliably identified *BCR-ABL1* B-ALL based on the receiving operating characteristic analysis. Dasatinib LC_{50} from 307 B-ALL (including 71 *BCR-ABL* B-ALL) was analyzed, and a LC_{50} cutoff at 80nM achieved the optimal balance in sensitivity and specificity that distinguishes *BCR-ABL* samples from other B-ALLs. **D.** Examples of dose-response curve of dasatinib-sensitive or -resistant B-ALL and T-ALL. Sensitive and resistant cases are shown in red and blue, respectively. The sensitive B-ALL sample is *BCR-ABL1*-positive. For each patient at each drug concentration, cells were tested in duplicates. **E.** Of drugs tested for at least 30 cases in the T-ALL cohorts, LC_{50} of prednisolone and asparaginase

exhibited a bimodal distribution whereas 6-MP and daunorubicin did not. N=43, 38, 40, and 41 patients for prednisone, daunorubicin, 6-MP, and L-Asparaginase, respectively.

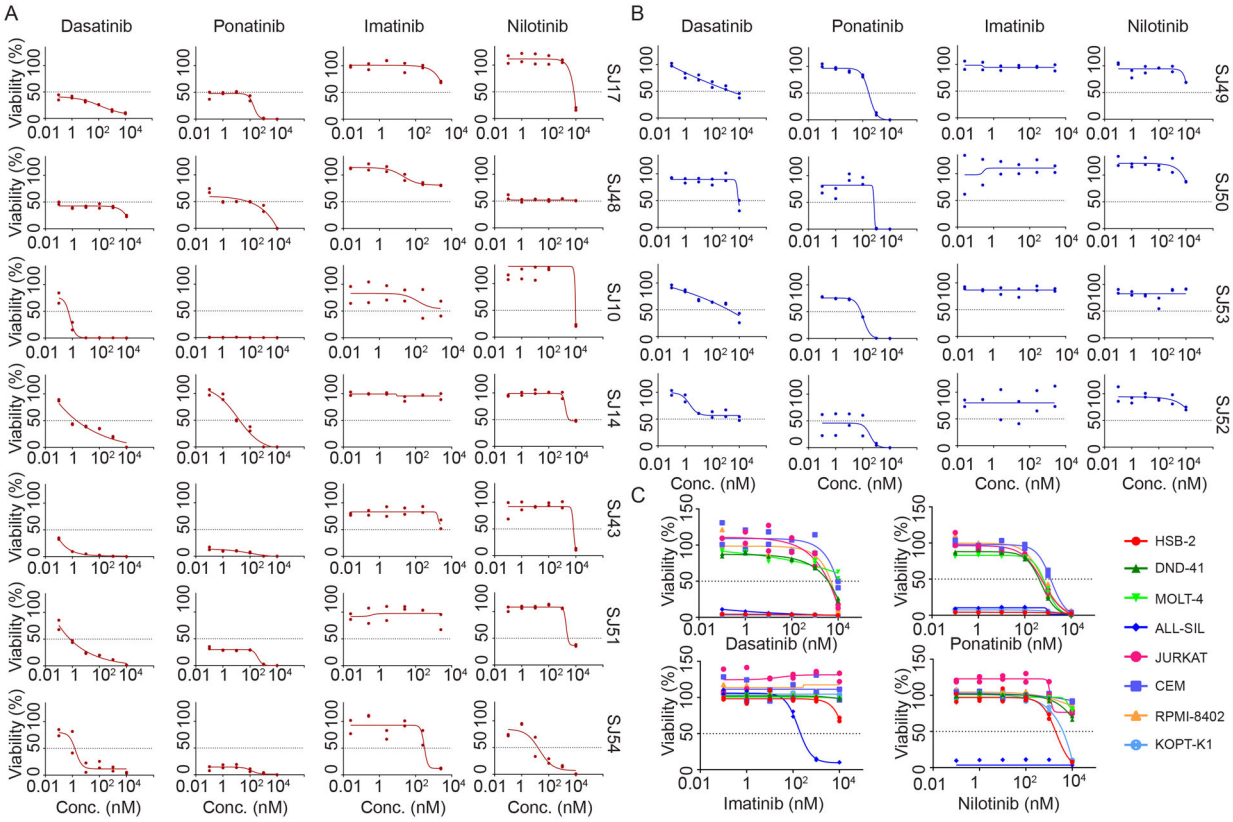

Extended Data Fig. 2. Comparison of T-ALL sensitivity to four ABL inhibitors.

A-B. PDX-derived leukemia cells were tested for sensitivity to each of the 4 inhibitors. A total of 11 cases were selected to represent dasatinib-sensitive vs resistant T-ALL and were xenografted in NSG mice to develop PDX. Mice were sacrificed once leukemia burden reached predefined endpoint, and human leukemia cells were harvested and subjected to drug sensitivity profiling *ex vivo*. Cells were incubated with increasing concentrations of each ABL inhibitor for 96 hours and cell viability was determined by flow cytometry as described in Methods. **C.** Dose-dependent cell death was determined for four ABL inhibitors in 8 T-ALL cell lines. HSB-2 (harbors *TCR-LCK* fusion), KOPT-K1 (harbors *TCR-LMO2* fusion) and ALL-SIL (harbors ABL class fusion) were sensitive (LC_{50}s are less than 0.05 nM) to both dasatinib and ponatinib but resistant to imatinib and nilotinib. For each leukemia case at each drug concentration, cells were tested in duplicates.

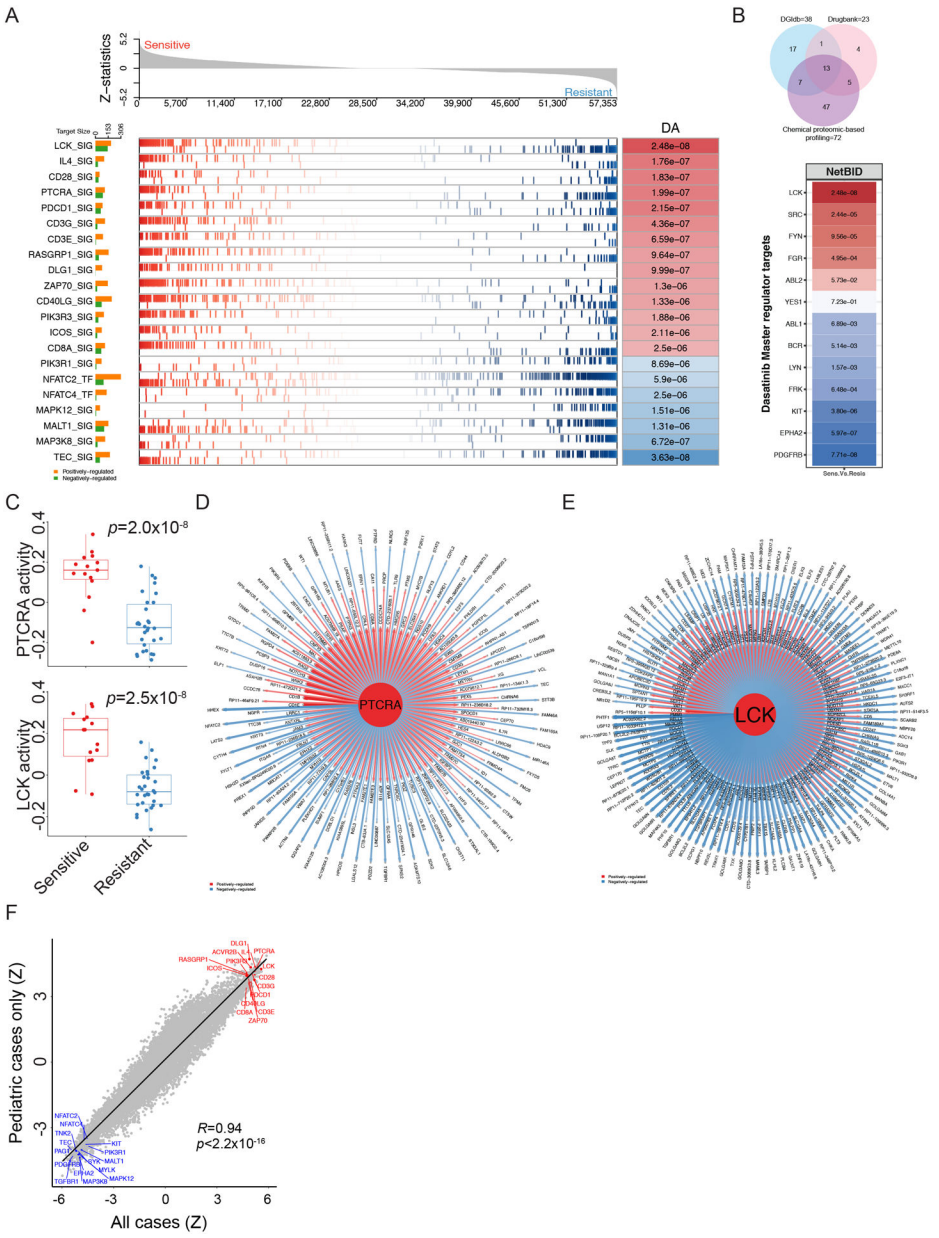

Extended Data Fig. 3. NetBID identified LCK and related genes for association with dasatinib sensitivity in T-ALL.

A. Activity of each gene was inferred using NetBID as described in Method and then compared between dasatinib-sensitive vs -resistant T-ALL with P value listed in the far right column. Top panel describes the expression ranking of all genes from the most highly expressed in dasatinib-sensitive cases on the left to the most highly expressed in resistant T-ALL on the right. Each gene in this pathway regulates a multitude of targets and their expression is indicated in two rows with positive-regulated target genes on the top and negatively regulated target genes at the bottom. In the case of LCK, it has 188 positive and 147 negative targets, each represented by a vertical line. Red lines indicate high expression in dasatinib sensitive T-ALL and blue lines indicate high expression in dasatinib-resistant cases. P-value was estimated using two-tailed t test. **B.** NetBID results for dasatinib target

genes for association with dasatinib sensitivity in T-ALL. Dasatinib target gene list is derived from three databases Drug Bank, DGIdb, and chemical proteomic-based TKI target profiling, as shown in the Venn diagram in the left panel. Thirteen targets are commonly identified across three sources. NetBID analysis identified four of these 13 targets with a significantly higher activity (LCK, SRC, FYN and FGR) in dasatinib-sensitive samples compared to resistant cases, with P value for the differential gene activity listed in the right panel. P-value was estimated using two-tailed t test. **C.** PTCRA and LCK activity were compared between dasatinib-sensitive vs -resistant T-ALL samples with RNA-seq data in the pharmacotyping cohort (N=15 and 30, respectively), P-value was estimated using two-tailed t test. Boxplots show summary of data in terms of the minimum, maximum, sample median, and the first and third quartiles. **D-E**, Gene networks used to infer PTCRA (**D**) and LCK (**E**) activity in NetBID. Each spoke represents a target gene (positively-regulated as red and negatively-regulated as blue), with gene name indicated at the edge of each arrow. P-value was estimated using two-tailed t test. **F.** Running NetBID analysis using only pediatric cases in the discovery cohort (N=12 and 15 patients for dasatinib-sensitive and -resistant, respectively), we re-estimated Z score for each gene which were then correlated with those from NetBID analysis using all T-ALL cases. Genes in the 30 biomarker panel are labeled and P value was estimated using Pearson correlation test.

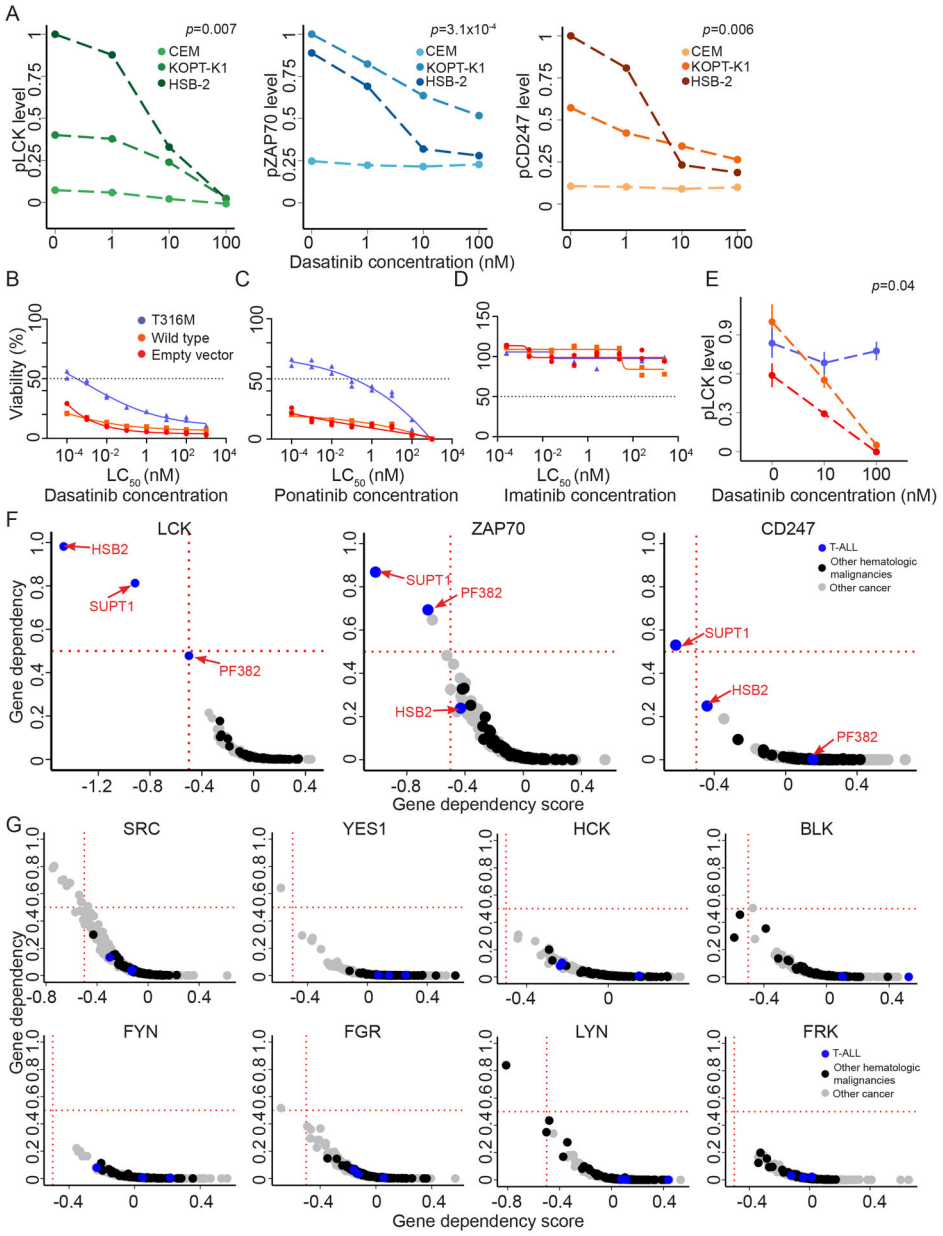

Extended Data Fig. 4. LCK signaling is essential for dasatinib sensitivity in T-ALL.

A. Phospho-flow of LCK, ZAP70 and CD247 in dasatinib-sensitive vs -resistant T-ALL cell lines. Cells were treated with increasing concentrations of dasatinib for 1 hour and then subjected to intracellular staining for phosphorylated LCK, ZAP70, and CD247, as described in Method. Phospho-protein was quantified by flow cytometry and normalized with samples not exposed to dasatinib as 100%. HSB-2 and KOPT-K1 (sensitive to dasatinib) is plotted in darker colors while CEM (resistant) is plotted in lighter colors. P-values were derived by ANOVA. **B-D.** LCK T316M mutation confers dasatinib resistance in KOPT-K1 cells. LCK T316M mutation was ectopically expressed in dasatinib-sensitive T-ALL KOPT-K1 cells. KOPT-K1 cells with wildtype LCK overexpression or empty vector control remained sensitive to dasatinib and ponatinib while overexpression of T316M LCK

resulted in resistance to dasatinib (**B**) and ponatinib (**C**). Meanwhile, all three lines were resistant to ABL specific inhibitor imatinib (**D**). For each leukemia sample at each drug concentration, cells were tested in duplicates. **E**. In KOPT-K1 cells with expressing wildtype LCK or empty vector control, LCK phosphorylation was inhibited by dasatinib in a dose-dependent manner, whereas LCK phosphorylation was unablated by dasatinib in cells expressing the T136M mutant LCK. Standard deviation is derived from biologically independent samples (N=3) and is plotted as error bar. P value was estimated using Wilcoxon test. **F-G.** Genome-wide CRISPR screen identifies preTCR pathway genes as dependencies in T-ALL. **F.** LCK, ZAP70 and CD247 dependency score (x-axis) versus gene dependency probability (y-axis) demonstrates that a subset of T-ALL lines (blue, N=3) show dependency on these preTCR pathway genes compared to all other cell lines screened (hematologic cancer cell lines in black, N=73 and other cancer cell lines in gray, N=613). Gene dependency of greater than 0.5 indicates a high probability that a cell line is dependent and corresponds to an approximate dependency score of −0.5. More negative gene dependency scores indicate greater effect on cell line survival. **G.** Gene dependency score (x-axis) versus gene dependency probability (y-axis) demonstrates that none of the T-ALL lines (blue, N=3) show dependency on SRC kinase family genes (other than LCK show in Fig. 2J) compared to all other cell lines screened (hematologic cancer cell lines in black, N=73 and other cancer cell lines in gray, N=613). Gene dependency of greater than 0.5 indicates a high probability that a cell line is dependent and corresponds to an approximate dependency score of −0.5. More negative gene dependency scores indicate greater effect on cell line survival.

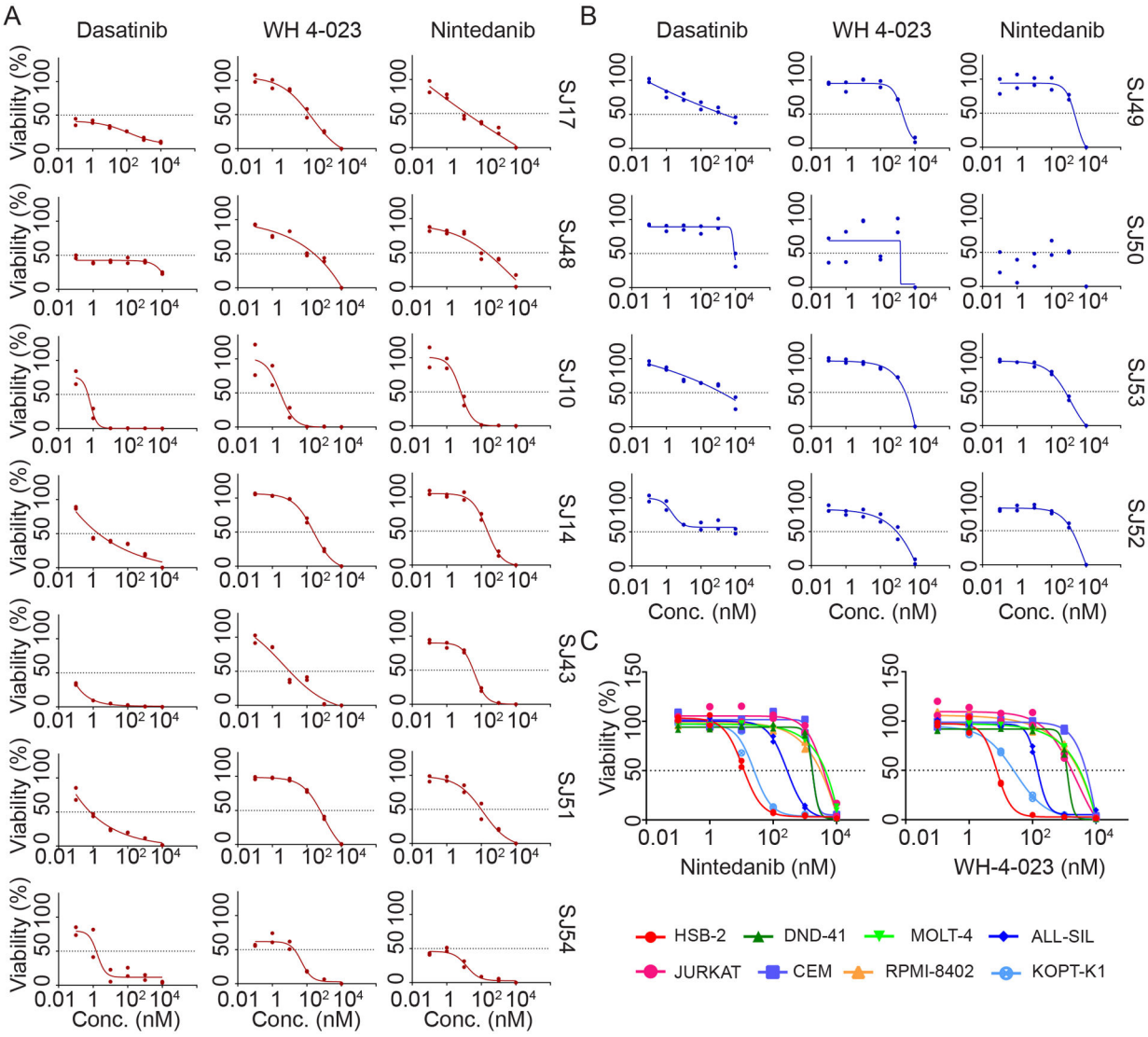

Extended Data Fig. 5. Comparison of T-ALL sensitivity to three LCK inhibitors.

A-B. A total of 11 cases were selected to represent dasatinib-sensitive vs resistant T-ALL (N=7 and 4 in Panels **A** and **B**, respectively) and were xenografted in NSG mice to develop PDX. Mice were sacrificed once leukemia burden reached predefined endpoint, and human leukemia cells were harvested and subjected to drug sensitivity profiling *ex vivo*. Cells were incubated with increasing concentrations of each LCK inhibitor for 96 hours and cell viability was determined by flow cytometry as described in Methods**. C.** Dose-dependent cell death was determined for two drugs in 8 T-ALL cell lines. For both drugs, HSB-2, (harbors *TCR-LCK* fusion) and KOPT-K1 (harbors *TCR-LMO2* fusion) showed the highest sensitivity compared to ALL-SIL (harbors ABL class fusion) and other T-ALL cell lines. For each leukemia sample at each drug concentration, cells were tested in duplicates.

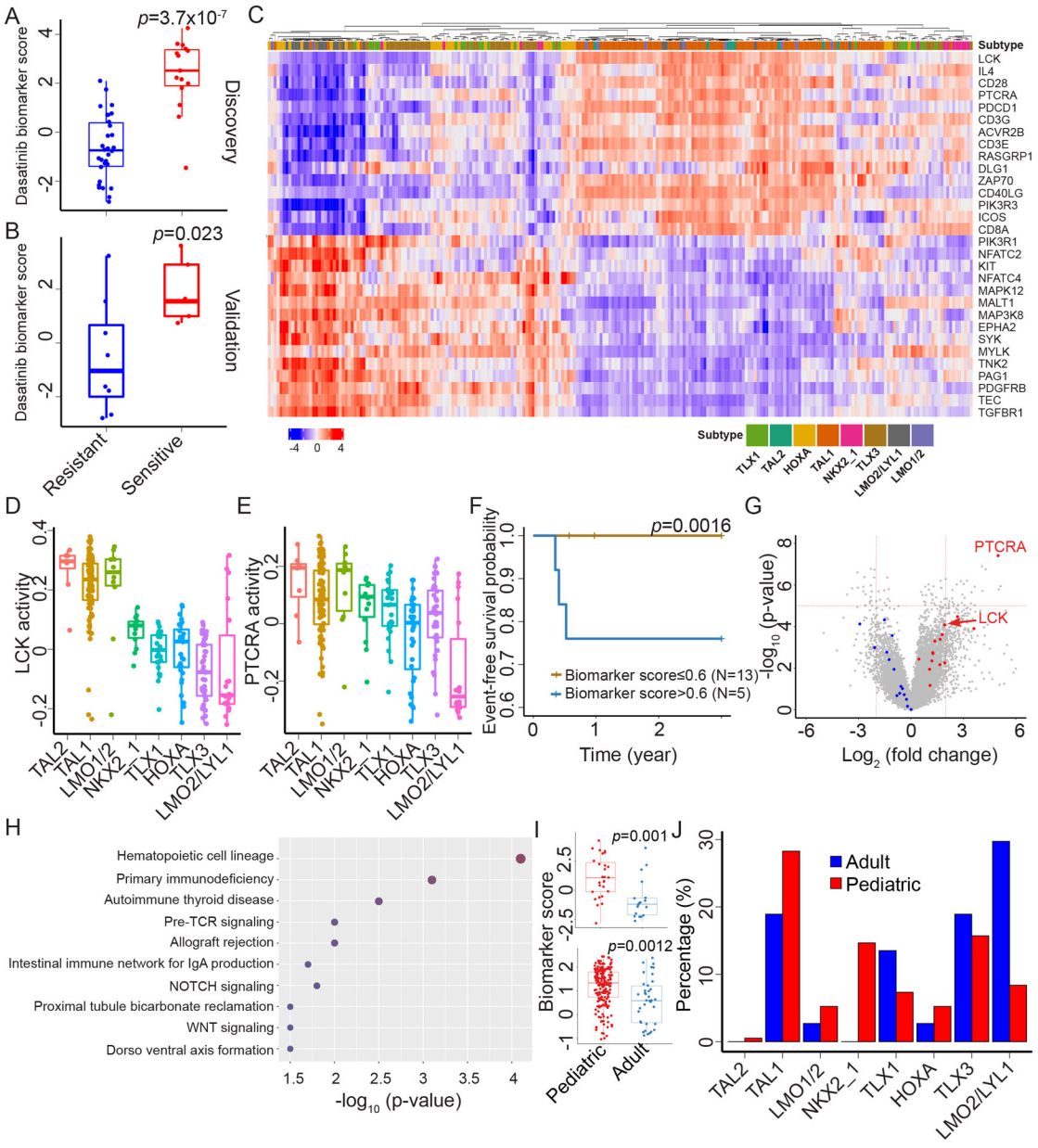

Extended Data Fig. 6. Biomarker model of dasatinib sensitivity in T-ALL.

A-B. A panel of 30 genes were selected as biomarkers from the top 461 driver genes in the NetBID analysis, as described in Methods. Dasatinib biomarker score was plotted for T-ALL cases, in the discovery cohort (**A**, N=45) and in the validation cohort (**B**, N=13). P value was estimated using two-tailed t test. **C.** Similarly, activity of each biomarker gene was estimated for the TARGET T-ALL cohort, from which an unsupervised clustering analysis was performed, as shown in the heatmap. Each row is a biomarker gene and each column represents a T-ALL case, with color discriminating the level of inferred gene activity. T-ALL subtype is indicated in the top row by color. **D-E.** Predicted LCK and PTCRA activity in the TARGET T-ALL cohort (N=261) using the biomarker model. Activity of LCK and PTCRA was estimated for each T-ALL case from its RNA-seq data by NetBID algorithm. T-ALL

subtypes were defined as previously described (Liu *et al.*, 2017). **F.** In TARGET cohort, dasatinib biomarker score of cases in *LMO2/LYL1* subtype showed a bimodal distribution. Cases with high biomarker score (dasatinib-sensitive, blue curve) exhibited a worse event-free survival compared to those with low biomarker score. P-value was estimated using Cox regression. **G-H.** Differential gene expression analyses of dasatinib sensitivity in T-ALL. In the discovery cohort, differences in gene expression between dasatinib-sensitive vs -resistant T-ALL was examined using the Limma method based on a linear model and results are presented as the volcano plot compared (**G**). Pathway analysis was performed with 254 genes that met the significance and effect size threshold (adjusted P<1e-3 and log2 fold change >2), using the KEGG pathway database. P-value was inferred by Fisher exact test. **I-J.** Comparison of predicted dasatinib sensitivity in pediatric and adult T-ALL. **I.** Dasatinib biomarker score was significantly higher in pediatric cases than adults in the discovery cohort. This was also validated in an independent microarray-based T-ALL gene expression dataset (NCBI GSE32215) with 37 adult and 191 pediatric patient samples. **J**.T-ALL subtype was inferred from gene expression profile for cases in the GSE32215 dataset. Pediatric cases have a higher prevalence of the TAL1 and TAL2 subtypes whereas adults have a higher frequency of HOXA and LMO2/LYL1 subtypes. P value was estimated using two-tailed t test. Boxplots show summary of data in terms of the minimum, maximum, sample median, and the first and third quartiles.

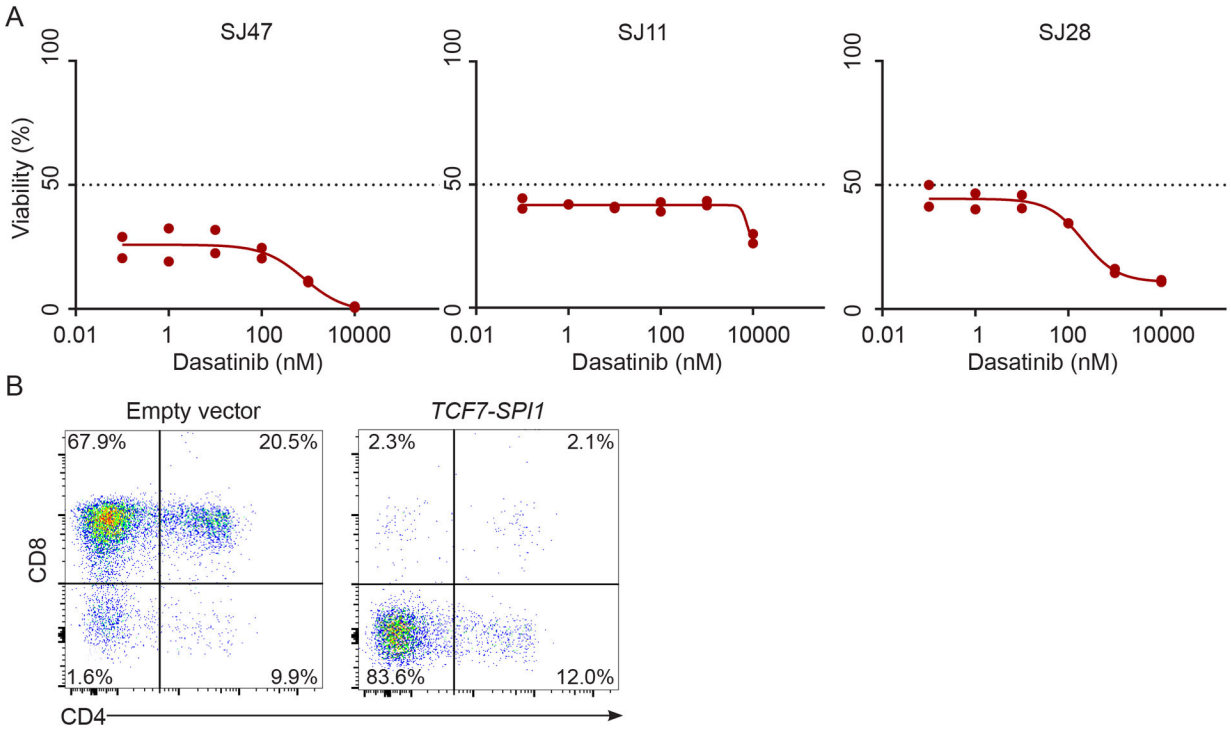

Extended Data Fig. 7. *SPI1*-rearrangement is associated with developmental arrest and related to dasatinib sensitivity in T-ALL.

A. Dose-dependent cell death was determined for dasatinib using the *ex vivo* drug sensitivity assay as described in Methods. For each patient at each drug concentration, cells were tested in duplicates. **B.** Mouse Lin-Sca+Ckit+ (LSK) cells were isolated from bone marrow and

transduced lentivirally with *SPI1* fusion gene or empty vector. After *in vitro* differentiation in the presence of OP9-DL1 cells and Il7 and Flt3 ligand, LSK cells were subjected to flow-cytometry analysis. *TCF7-SPI1* expressing cells exhibited differentiation blockade at DN stage while the empty control cells were able to extensively differentiate to double positive and single positive stages.

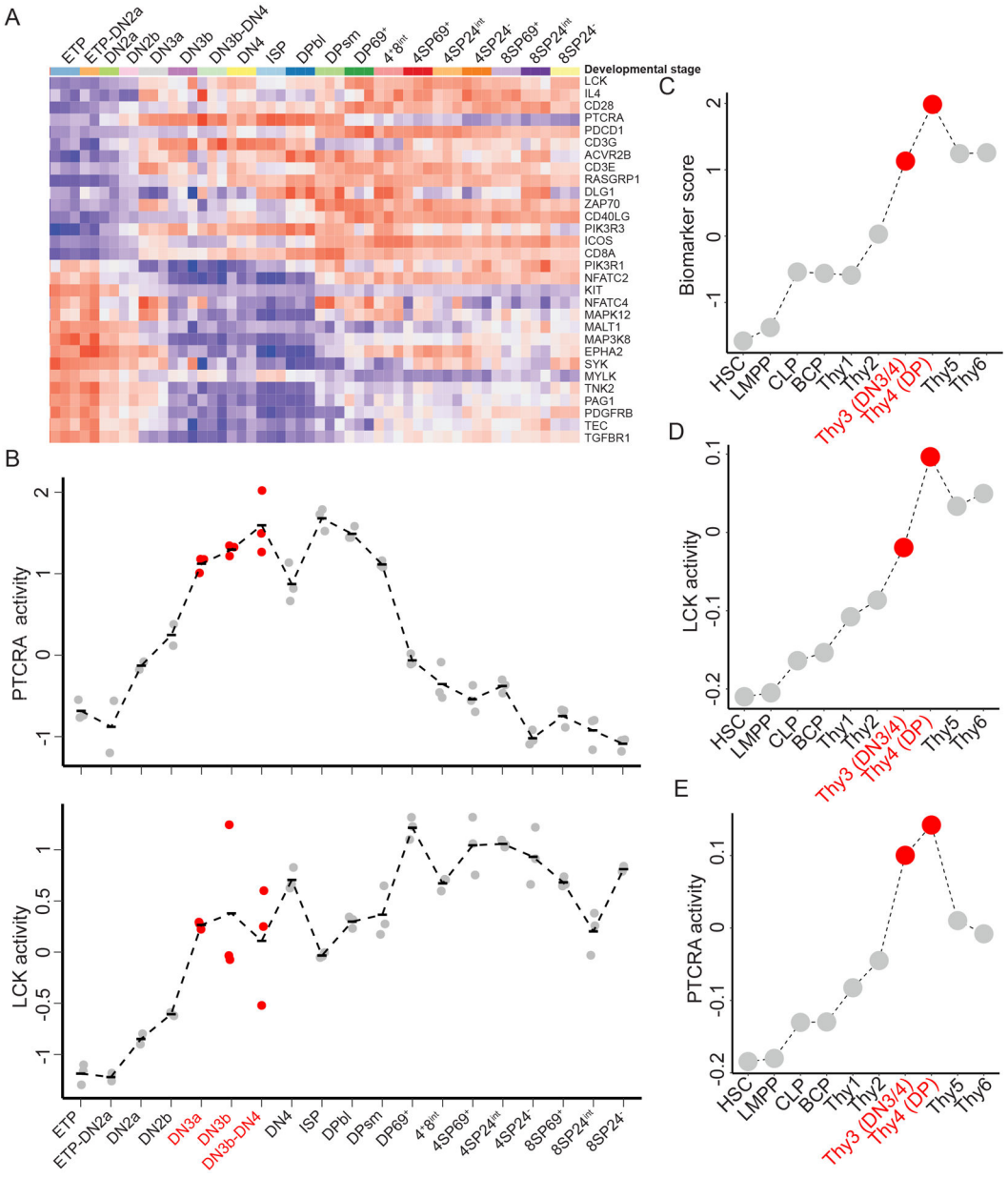

Extended Data Fig. 8. Activity of dasatinib sensitivity-related genes across normal T cell developmental stages in mouse and human.

A-B. The activity of dasatinib sensitivity genes vary by T cell differentiation stage in mouse. RNA-based gene expression profile was obtained from the previously published dataset (Mingueneau *et al.*, 2013), and NetBID was used to infer gene activity. **A.** NetBID-inferred activity of the 30 biomarker genes. Each mouse T cell developmental stage is represented as

a column and each row indicates different genes in the biomarker panel. Gene activity is represented by color (low to high as blue to red). **B.** NetBID-inferred activity of PTCRA and LCK. Horizontal bars indicate the mean of gene activity for each T cell population. DN3–4 stages are highlighted in red. **C-E.** NetBID-inferred dasatinib biomarker score and activity of PTCRA and LCK in 10 normal human T cell developmental stages. RNA-based gene expression profile of human T cells was obtained from the previously published dataset (Casero *et al.*, 2015). NetBID was used to infer LCK (**D**) and PTCRA (**E**) activity and biomarker score (**C**). Thy3 and Thy4 (approximately equivalent to DN3–4 and DN4 stages in mouse) are highlighted in red.

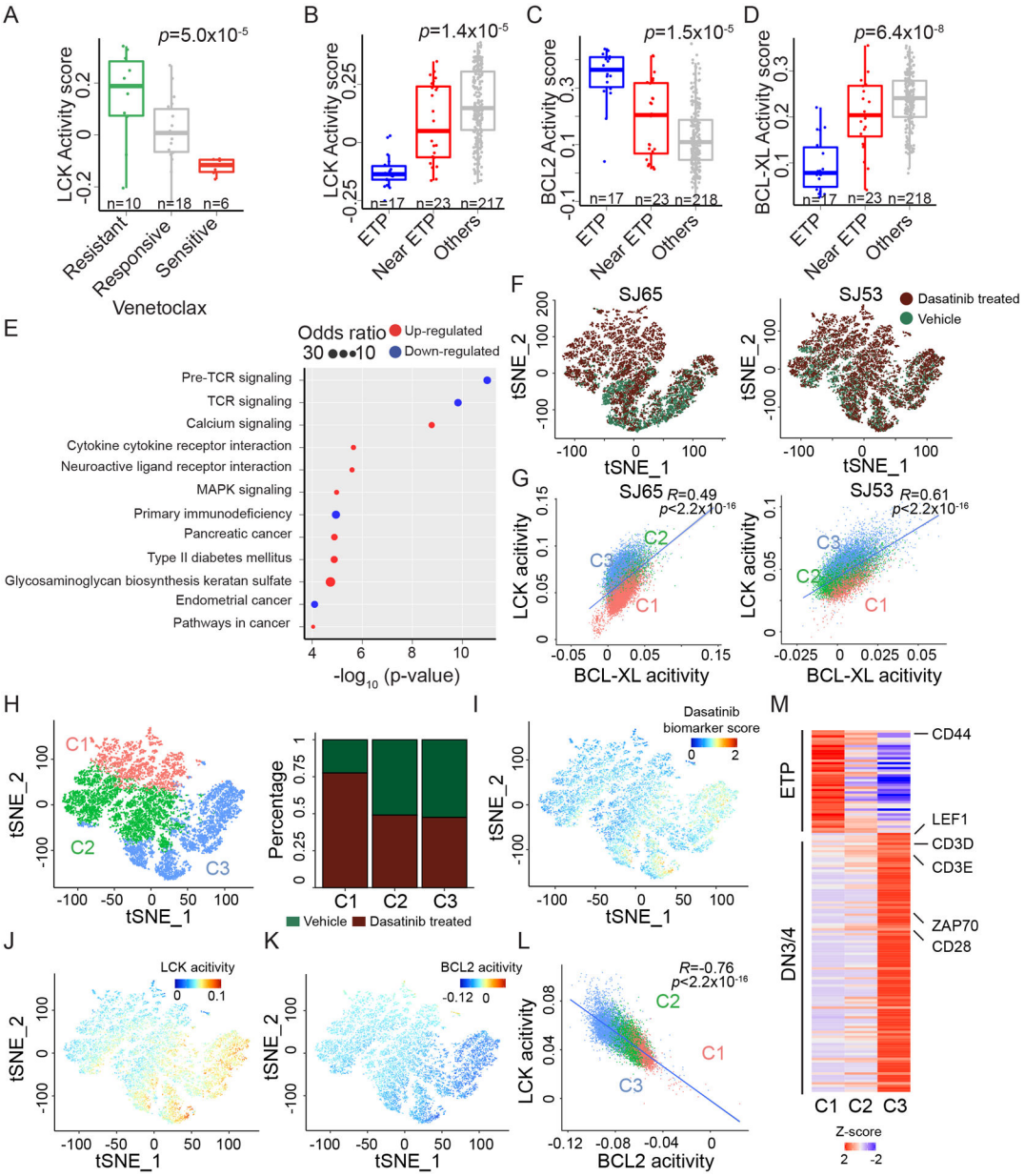

Extended Data Fig. 9. Relationship of LCK/BXL-XL/BCL2 activities with dasatinib and venetoclax sensitivity.

A. LCK activity was inversely correlated with venetoclax sensitivity *in vitro*. LCK activity was inferred from RNA-seq data using NetBID in the discovery cohort (P value was estimated using ANOVA). **B-D**. ETP T-ALL is associated with high BCL2 and low LCK/BCL-XL activity. BCL2/LCK/BCL-XL activity was estimated for cases in the TARGET cohort. Each case was annotated with ETP status. ETP cases exhibit low activity of LCK (**B**) and BCL-XL (**D**) while have high BCL2 activity (**C**). P-value was estimated using ANOVA. Boxplots show summary of data in terms of the minimum, maximum, sample median, and the first and third quartiles. **E.** NetBID analysis of venetoclax sensitivity in a subset of T-ALL case in the discovery cohort (N=34 patients) identified 656 driver genes for drug response. Genes in the Pre-TCR signaling pathway were most enriched in pathway analysis (downregulation linked to venetoclax sensitivity). **F-M.** Single cell transcriptomic analysis identified intra-leukemia heterogeneity in LCK activity. T-ALL cells from SJ53 were incubated with dasatinib or vehicle for 4 days in vitro. scRNA-seq was then performed using viable cells from each group separately but transcription profiling data was pooled for subsequent analyses. Vehicle-treated cells mimicked naïve and sensitive to dasatnib whereas cells survived dasatinib exposure (dasatinib-treated) represented drug resistant cell population. **F.** tSNE visualization shows the distribution of dasatinib-treated (brick red) and naïve (green) cells in SJ65 and SJ53. Single cell RNA-seq and data analyses were described in Methods. **G.** LCK and BCL-XL activity was inferred by NetBID from single cell RNA-seq of SJ66 and SJ53. P value were calculated using Pearson correlation, and color indicates cell populations (C1, C2, and C3 represented dasatinib resistant [red], responsive [green] and sensitive [blue] groups). P value was estimated using Pearson correlation. **H.** Left panel, unsupervised clustering analysis of scRNA-seq of vehicle and dasatinib-treated T-ALL cells from SJ53. Each dot represent a single cell visualized in a two-dimensional projection by t-SNE. Three clusters (C1, C2, and C3, in red, green, and blue, respectively) were identified using k-means clustering. Right panel, cell composition of each cluster is visualized by stack plot with red and green indicating the % of cells from vehicle or dasatinib-treated samples. C1, C2, and C3 consisted of increasing proportion of naïve dasatinib-sensitive cells, representing populations with low, intermediate, and high sensitivity to dasatinib, respectively. **I.** Distribution of Dasatinib biomarker score across three clusters. **J.** LCK activity was highest in cluster C3, intermediate in C2, and lowest in C1, paralleling the proportion of dasatinib-sensitive population. LCK activity is color-coded (from low to high, blue–red) on t-SNE plot. **K.** BCL2 activity was lowest in cluster C3, intermediate in C2, and highest in C1, paralleling the proportion of dasatinib-sensitive population. BCL2 activity is color-coded (from low to high, blue–red) on t-SNE plot. **L.** Inverse correlation of LCK and BCL2 activity at the single cell level in SJ53. Each dot represents a cell and color discriminate clusters C1, C2, and C3 (red, green, and blue, respectively). Correlation coefficient and P value were estimated using Pearson correlation. **M.** Differentiation stage of each population was projected by examining the gene expression signature characteristic of ETP or DN3/DN4 T cells. Signature was derived from differential expression analysis of mouse T cell expression dataset (Mingueneau et al., 2013). Heatmap indicates the average of each gene (rows) for cells within each cluster (columns), after Z-normalization.

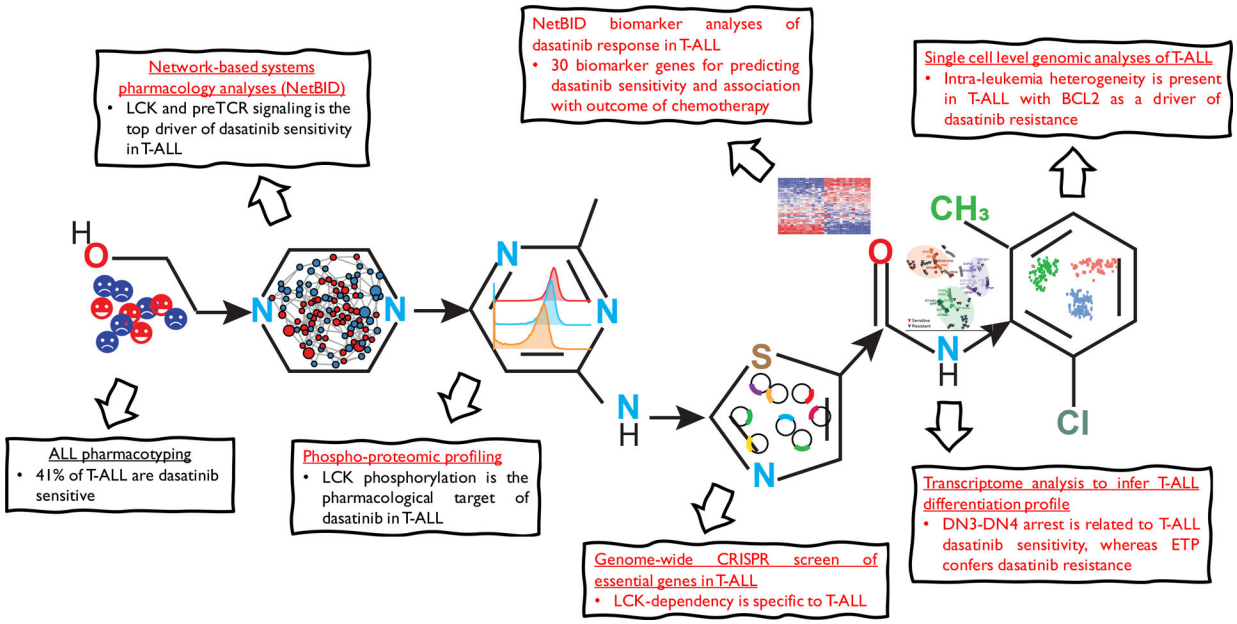

Extended Data Fig. 10. Schematic summary of main analyses, experiments, and major findings of this study.

Text is highlighted in red to indicate those unique to this report and advances compared to previous findings.

Supplementary Material

Refer to Web version on PubMed Central for supplementary material.

Acknowledgments

We thank the patients and families who participated in the clinical trials included in this study for donating specimens for research and the clinicians and research staff for assistance in sample collection, processing, and curation. We also thank Hannah Williams and Suiping Zhou for their assistance in the drug sensitivity profiling and phospho-proteomics profiling assays, respectively. We appreciate the thoughtful discussions with Dr. Takaomi Sanda at National University of Singapore. This work was in part supported by the National Institutes of Health (R35CA210030, R37CA36401, P50GM115279, R01GM118578, R01GM134382, P30CA21765), the St. Baldrick's Foundation, and the Pan-Mass Challenge Team Crank, and by the American Lebanese Syrian Associated Charities. Yoshihiro Gocho was supported by Tokyo Children's Cancer Study Group overseas scholarship and Nippon Medical School, Japan.

Competing interests Statement

K.S. currently has funding from Novartis International AG and previously consulted for Rigel Pharmaceuticals on topics unrelated to this manuscript. M.V.R. J.J.Y, and St. Jude receive investigatory-initiated research funding from Servier for work unrelated to this manuscript. J.J.Y and J.Y. are also named as co-inventors on a pending provisional U.S. patent application filed by St. Jude based on this research.

References

1. Pui CH et al. Childhood Acute Lymphoblastic Leukemia: Progress Through Collaboration. J Clin Oncol 33, 2938–48 (2015). [PubMed: 26304874]
2. Hunger SP & Mullighan CG Acute lymphoblastic leukemia in children. N Engl J Med 373, 1541–52 (2015). [PubMed: 26465987]

3. Slayton WB et al. Dasatinib Plus Intensive Chemotherapy in Children, Adolescents, and Young Adults With Philadelphia Chromosome-Positive Acute Lymphoblastic Leukemia: Results of Children's Oncology Group Trial AALL0622. J Clin Oncol 36, 2306–2314 (2018). [PubMed: 29812996]
4. Shen S et al. Effect of Dasatinib vs Imatinib in the Treatment of Pediatric Philadelphia Chromosome-Positive Acute Lymphoblastic Leukemia: A Randomized Clinical Trial. JAMA Oncol (2020).
5. Roberts KG et al. Targetable kinase-activating lesions in Ph-like acute lymphoblastic leukemia. N Engl J Med 371, 1005–15 (2014). [PubMed: 25207766]
6. Raetz EA & Teachey DT T-cell acute lymphoblastic leukemia. Hematology Am Soc Hematol Educ Program 2016, 580–588 (2016). [PubMed: 27913532]
7. Girardi T, Vicente C, Cools J & De Keersmaecker K The genetics and molecular biology of T-ALL. Blood 129, 1113–1123 (2017). [PubMed: 28115373]
8. Liu Y et al. The genomic landscape of pediatric and young adult T-lineage acute lymphoblastic leukemia. Nat Genet 49, 1211–1218 (2017). [PubMed: 28671688]
9. McMahon CM & Luger SM Relapsed T cell ALL: current approaches and new directions. Curr Hematol Malig Rep 14, 83–93 (2019). [PubMed: 30880359]
10. Nguyen K et al. Factors influencing survival after relapse from acute lymphoblastic leukemia: a Children's Oncology Group study. Leukemia 22, 2142–50 (2008). [PubMed: 18818707]
11. Teachey DT & Hunger SP Acute lymphoblastic leukaemia in 2017: Immunotherapy for ALL takes the world by storm. Nat Rev Clin Oncol 15, 69–70 (2018). [PubMed: 29255238]
12. Palomero T & Ferrando A Therapeutic targeting of NOTCH1 signaling in T-cell acute lymphoblastic leukemia. Clin Lymphoma Myeloma 9 Suppl 3, S205–10 (2009).
13. Sarmento LM & Barata JT Therapeutic potential of Notch inhibition in T-cell acute lymphoblastic leukemia: rationale, caveats and promises. Expert Rev Anticancer Ther 11, 1403–15 (2011). [PubMed: 21929314]
14. Takebe N, Nguyen D & Yang SX Targeting notch signaling pathway in cancer: clinical development advances and challenges. Pharmacol Ther 141, 140–9 (2014). [PubMed: 24076266]
15. Doody RS et al. A phase 3 trial of semagacestat for treatment of Alzheimer's disease. N Engl J Med 369, 341–50 (2013). [PubMed: 23883379]
16. Le Tourneau C et al. Molecularly targeted therapy based on tumour molecular profiling versus conventional therapy for advanced cancer (SHIVA): a multicentre, open-label, proof-of-concept, randomised, controlled phase 2 trial. Lancet Oncol 16, 1324–34 (2015). [PubMed: 26342236]
17. Sicklick JK et al. Molecular profiling of cancer patients enables personalized combination therapy: the I-PREDICT study. Nat Med 25, 744–750 (2019). [PubMed: 31011206]
18. Letai A Functional precision cancer medicine-moving beyond pure genomics. Nat Med 23, 1028–1035 (2017). [PubMed: 28886003]
19. Tyner JW et al. Functional genomic landscape of acute myeloid leukaemia. Nature 562, 526–531 (2018). [PubMed: 30333627]
20. Lee JK et al. Pharmacogenomic landscape of patient-derived tumor cells informs precision oncology therapy. Nat Genet 50, 1399–1411 (2018). [PubMed: 30262818]
21. Vlachogiannis G et al. Patient-derived organoids model treatment response of metastatic gastrointestinal cancers. Science 359, 920–926 (2018). [PubMed: 29472484]
22. Frismantas V et al. Ex vivo drug response profiling detects recurrent sensitivity patterns in drug-resistant acute lymphoblastic leukemia. Blood 129, e26–e37 (2017). [PubMed: 28122742]
23. Snijder B et al. Image-based ex-vivo drug screening for patients with aggressive haematological malignancies: interim results from a single-arm, open-label, pilot study. Lancet Haematol 4, e595–e606 (2017). [PubMed: 29153976]
24. Holleman A et al. Gene-expression patterns in drug-resistant acute lymphoblastic leukemia cells and response to treatment. N Engl J Med 351, 533–42 (2004). [PubMed: 15295046]
25. Diouf B et al. Somatic deletions of genes regulating MSH2 protein stability cause DNA mismatch repair deficiency and drug resistance in human leukemia cells. Nat Med 17, 1298–303 (2011). [PubMed: 21946537]

26. Putcha P et al. HDAC6 activity is a non-oncogene addiction hub for inflammatory breast cancers. Breast Cancer Research 17, 149 (2015). [PubMed: 26643555]
27. Alvarez MJ et al. A precision oncology approach to the pharmacological targeting of mechanistic dependencies in neuroendocrine tumors. Nature Genetics 50, 979–989 (2018). [PubMed: 29915428]
28. Piovan E et al. Direct Reversal of Glucocorticoid Resistance by AKT Inhibition in Acute Lymphoblastic Leukemia. Cancer Cell 24, 766–776 (2013). [PubMed: 24291004]
29. Kantarjian H, Jabbour E, Grimley J & Kirkpatrick P Dasatinib. Nature Reviews Drug Discovery 5, 717–718 (2006).
30. Greuber EK, Smith-Pearson P, Wang J & Pendergast AM Role of ABL family kinases in cancer: from leukaemia to solid tumours. Nat Rev Cancer 13, 559–71 (2013). [PubMed: 23842646]
31. Nam S et al. Action of the Src Family Kinase Inhibitor, Dasatinib (BMS-354825), on Human Prostate Cancer Cells. Cancer Research 65, 9185–9189 (2005). [PubMed: 16230377]
32. Ceppi P et al. Effects of Src kinase inhibition induced by dasatinib in non–small cell lung cancer cell lines treated with cisplatin. Molecular Cancer Therapeutics 8, 3066–3074 (2009). [PubMed: 19861409]
33. Serafin V et al. Glucocorticoid resistance is reverted by LCK inhibition in pediatric T-cell acute lymphoblastic leukemia. Blood 130, 2750–2761 (2017). [PubMed: 29101238]
34. Laukkanen S et al. In silico and preclinical drug screening identifies dasatinib as a targeted therapy for T-ALL. Blood Cancer Journal 7, e604–e604 (2017). [PubMed: 28885610]
35. Shi Y et al. Phase II-like murine trial identifies synergy between dexamethasone and dasatinib in T-cell acute lymphoblastic leukemia. Haematologica, haematol.2019.241026 (2020).
36. Kim De K et al. NUP214-ABL1-mediated cell proliferation in T-cell acute lymphoblastic leukemia is dependent on the LCK kinase and various interacting proteins. Haematologica 99, 85–93 (2014). [PubMed: 23872305]
37. Du X et al. Hippo/Mst signalling couples metabolic state and immune function of CD8α+ dendritic cells. Nature 558, 141–145 (2018). [PubMed: 29849151]
38. Khatamian A, Paull EO, Califano A & Yu J SJARACNe: a scalable software tool for gene network reverse engineering from big data. Bioinformatics 35, 2165–2166 (2019). [PubMed: 30388204]
39. Wishart DS et al. DrugBank 5.0: a major update to the DrugBank database for 2018. Nucleic Acids Research 46, D1074–D1082 (2017).
40. Cotto KC et al. DGIdb 3.0: a redesign and expansion of the drug–gene interaction database. Nucleic Acids Research 46, D1068–D1073 (2017).
41. Klaeger S et al. The target landscape of clinical kinase drugs. Science 358, eaan4368 (2017). [PubMed: 29191878]
42. Nyakeriga AM, Garg H & Joshi A TCR-induced T cell activation leads to simultaneous phosphorylation at Y505 and Y394 of p56(lck) residues. Cytometry A 81, 797–805 (2012). [PubMed: 22674786]
43. Weber EW et al. Pharmacologic control of CAR-T cell function using dasatinib. Blood Adv 3, 711–717 (2019). [PubMed: 30814055]
44. Williams BL et al. Phosphorylation of Tyr319 in ZAP-70 is required for T-cell antigen receptor-dependent phospholipase C-gamma1 and Ras activation. EMBO J 18, 1832–44 (1999). [PubMed: 10202147]
45. Lee KC et al. Lck is a key target of imatinib and dasatinib in T-cell activation. Leukemia 24, 896–900 (2010). [PubMed: 20147973]
46. Martin MW et al. Novel 2-aminopyrimidine carbamates as potent and orally active inhibitors of Lck: synthesis, SAR, and in vivo antiinflammatory activity. J Med Chem 49, 4981–91 (2006). [PubMed: 16884310]
47. Roth GJ et al. Nintedanib: From Discovery to the Clinic. Journal of Medicinal Chemistry 58, 1053–1063 (2015). [PubMed: 25474320]
48. Seki M et al. Recurrent SPI1 (PU.1) fusions in high-risk pediatric T cell acute lymphoblastic leukemia. Nature Genetics 49, 1274–1281 (2017). [PubMed: 28671687]

49. Rothenberg EV, Moore JE & Yui MA Launching the T-cell-lineage developmental programme. Nature Reviews Immunology 8, 9–21 (2008).
50. Mingueneau M et al. The transcriptional landscape of αβ T cell differentiation. Nature Immunology 14, 619–632 (2013). [PubMed: 23644507]
51. Chonghaile TN et al. Maturation Stage of T-cell Acute Lymphoblastic Leukemia Determines BCL-2 versus BCL-XL Dependence and Sensitivity to ABT-199. Cancer Discovery 4, 1074–1087 (2014). [PubMed: 24994123]
52. Bellavia D et al. Combined expression of pTalpha and Notch3 in T cell leukemia identifies the requirement of preTCR for leukemogenesis. Proc Natl Acad Sci U S A 99, 3788–93 (2002). [PubMed: 11891328]
53. dos Santos NR et al. Pre-TCR expression cooperates with TEL-JAK2 to transform immature thymocytes and induce T-cell leukemia. Blood 109, 3972–81 (2007). [PubMed: 17192390]
54. Yamasaki S & Saito T Molecular basis for pre-TCR-mediated autonomous signaling. Trends Immunol 28, 39–43 (2007). [PubMed: 17126602]
55. Chao DT et al. Bcl-XL and Bcl-2 repress a common pathway of cell death. Journal of Experimental Medicine 182, 821–828 (1995).
56. Gratiot-Deans J, Merino R, Nuñez G & Turka LA Bcl-2 expression during T-cell development: early loss and late return occur at specific stages of commitment to differentiation and survival. Proceedings of the National Academy of Sciences 91, 10685–10689 (1994).
57. Jeha S et al. Improved CNS Control of Childhood Acute Lymphoblastic Leukemia Without Cranial Irradiation: St Jude Total Therapy Study 16. Journal of Clinical Oncology 37, 3377–3391 (2019). [PubMed: 31657981]
58. Zwaan CM et al. Dasatinib in Children and Adolescents With Relapsed or Refractory Leukemia: Results of the CA180–018 Phase I Dose-Escalation Study of the Innovative Therapies for Children With Cancer Consortium. Journal of Clinical Oncology 31, 2460–2468 (2013). [PubMed: 23715577]
59. Aplenc R et al. Pediatric Phase I Trial and Pharmacokinetic Study of Dasatinib: A Report From the Children's Oncology Group Phase I Consortium. Journal of Clinical Oncology 29, 839–844 (2011). [PubMed: 21263099]
60. Broniscer A et al. Phase I Trial, Pharmacokinetics, and Pharmacodynamics of Vandetanib and Dasatinib in Children with Newly Diagnosed Diffuse Intrinsic Pontine Glioma. Clinical Cancer Research 19, 3050–3058 (2013). [PubMed: 23536435]
61. Qian M et al. Whole-transcriptome sequencing identifies a distinct subtype of acute lymphoblastic leukemia with predominant genomic abnormalities of EP300 and CREBBP. Genome Research 27, 185–195 (2017). [PubMed: 27903646]
62. Zhang J et al. Germline Mutations in Predisposition Genes in Pediatric Cancer. New England Journal of Medicine 373, 2336–2346 (2015).
63. Rusch M et al. Clinical cancer genomic profiling by three-platform sequencing of whole genome, whole exome and transcriptome. Nat Commun 9, 3962 (2018). [PubMed: 30262806]
64. Chen X et al. CONSERTING: integrating copy-number analysis with structural-variation detection. Nature Methods 12, 527–530 (2015). [PubMed: 25938371]
65. Wang J et al. CREST maps somatic structural variation in cancer genomes with base-pair resolution. Nature Methods 8, 652–654 (2011). [PubMed: 21666668]
66. Pounds S et al. Reference alignment of SNP microarray signals for copy number analysis of tumors. Bioinformatics 25, 315–21 (2009). [PubMed: 19052058]
67. Iwamoto S, Mihara K, Downing JR, Pui CH & Campana D Mesenchymal cells regulate the response of acute lymphoblastic leukemia cells to asparaginase. J Clin Invest 117, 1049–57 (2007). [PubMed: 17380207]
68. Meyers RM et al. Computational correction of copy number effect improves specificity of CRISPR–Cas9 essentiality screens in cancer cells. Nature Genetics 49, 1779–1784 (2017). [PubMed: 29083409]
69. Dempster JM et al. Extracting Biological Insights from the Project Achilles Genome-Scale CRISPR Screens in Cancer Cell Lines. bioRxiv, 720243 (2019).

70. Benjamini Y & Hochberg Y Controlling the False Discovery Rate: A Practical and Powerful Approach to Multiple Testing. Journal of the Royal Statistical Society. Series B (Methodological) 57, 289–300 (1995).

71. Kanehisa M & Goto S KEGG: Kyoto Encyclopedia of Genes and Genomes. Nucleic Acids Research 28, 27–30 (2000). [PubMed: 10592173]

72. Piovan E et al. Direct reversal of glucocorticoid resistance by AKT inhibition in acute lymphoblastic leukemia. Cancer Cell 24, 766–76 (2013). [PubMed: 24291004]

73. Smedley D et al. BioMart--biological queries made easy. BMC Genomics 10, 22 (2009). [PubMed: 19144180]

74. Casero D et al. Long non-coding RNA profiling of human lymphoid progenitor cells reveals transcriptional divergence of B cell and T cell lineages. Nature Immunology 16, 1282–1291 (2015). [PubMed: 26502406]

75. Wang H et al. Deep multiomics profiling of brain tumors identifies signaling networks downstream of cancer driver genes. Nature Communications 10, 3718 (2019).

76. Hornbeck PV et al. PhosphoSitePlus: a comprehensive resource for investigating the structure and function of experimentally determined post-translational modifications in man and mouse. Nucleic Acids Research 40, D261–D270 (2011). [PubMed: 22135298]

77. Zhang J et al. FLT3 pathway is a potential therapeutic target for PRC2-mutated T-cell acute lymphoblastic leukemia. Blood 132, 2520–2524 (2018). [PubMed: 30282797]

78. Kiselev VY et al. SC3: consensus clustering of single-cell RNA-seq data. Nature methods 14, 483–486 (2017). [PubMed: 28346451]

79. Holleman A et al. Gene-Expression Patterns in Drug-Resistant Acute Lymphoblastic Leukemia Cells and Response to Treatment. New England Journal of Medicine 351, 533–542 (2004).

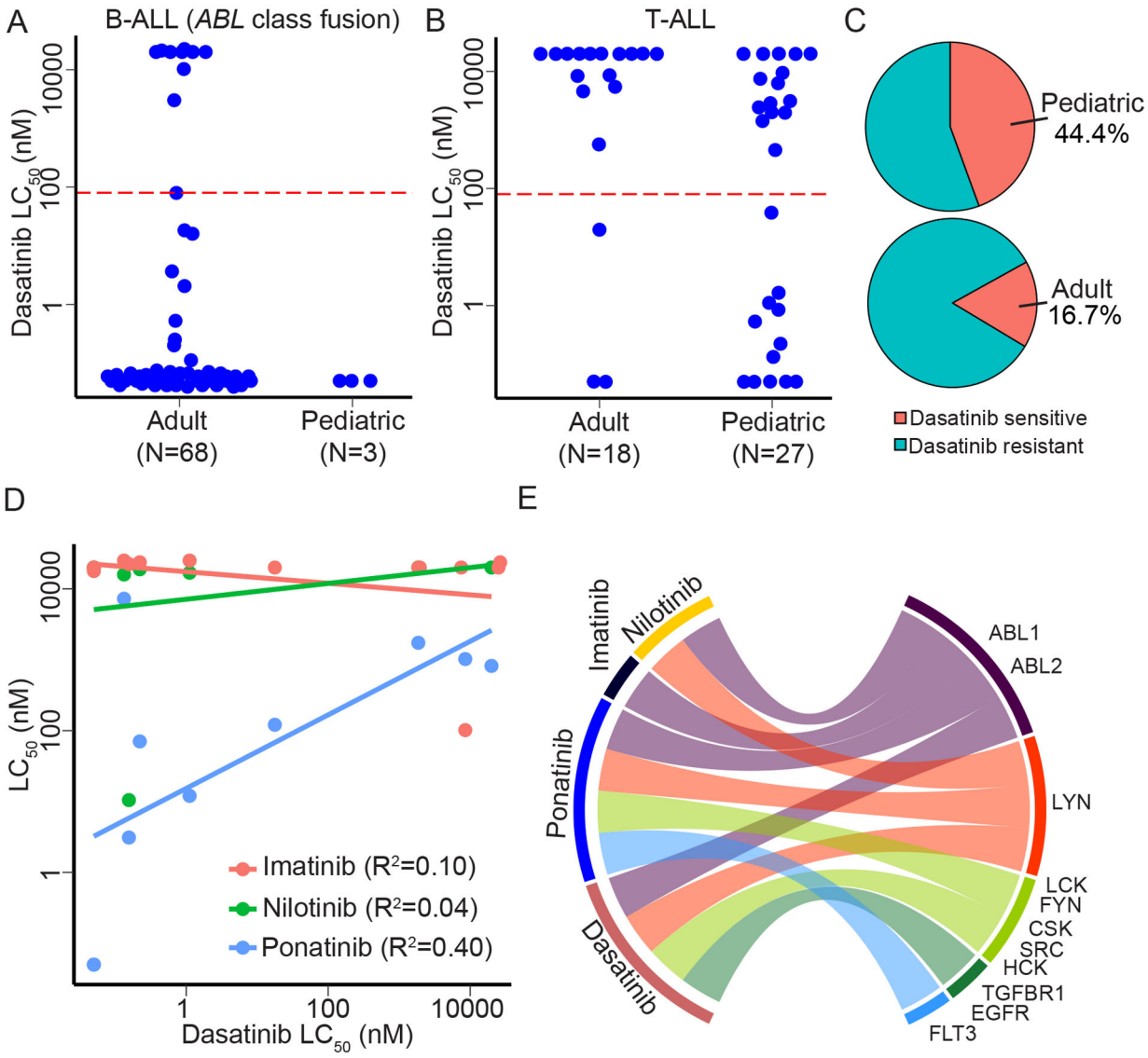

Figure 1. *Ex vivo* pharmacotyping identified dasatinib-sensitive T-ALL.

A and **B**, dasatinib LC_{50} distribution in *BCR-ABL1* B-ALL or those with *ABL* class fusions (N=71) and T-ALL (N=45). **C.** The proportion of dasatinib-sensitive T-ALL (marked in red) is significantly higher in children (44.4%) than in adults (16.7%). **D.** Comparison of dasatinib sensitivity with that to three other ABL inhibitors: imatinib (N=18), nilotinib (N=8) and ponatinib (N=10). LC_{50} correlation between each pair was evaluated using Spearman test. **E.** Circos plot of targets of four ABL inhibitors. TKIs (left) are connected to their purported targets (right), based on drug-target relationships previously described using systematic chemical proteomic profiling (Klaeger *et al.*, 2017). The right half of the circle highlights the shared targets across these four inhibitors. For all the above panels, N represents the number of patients.

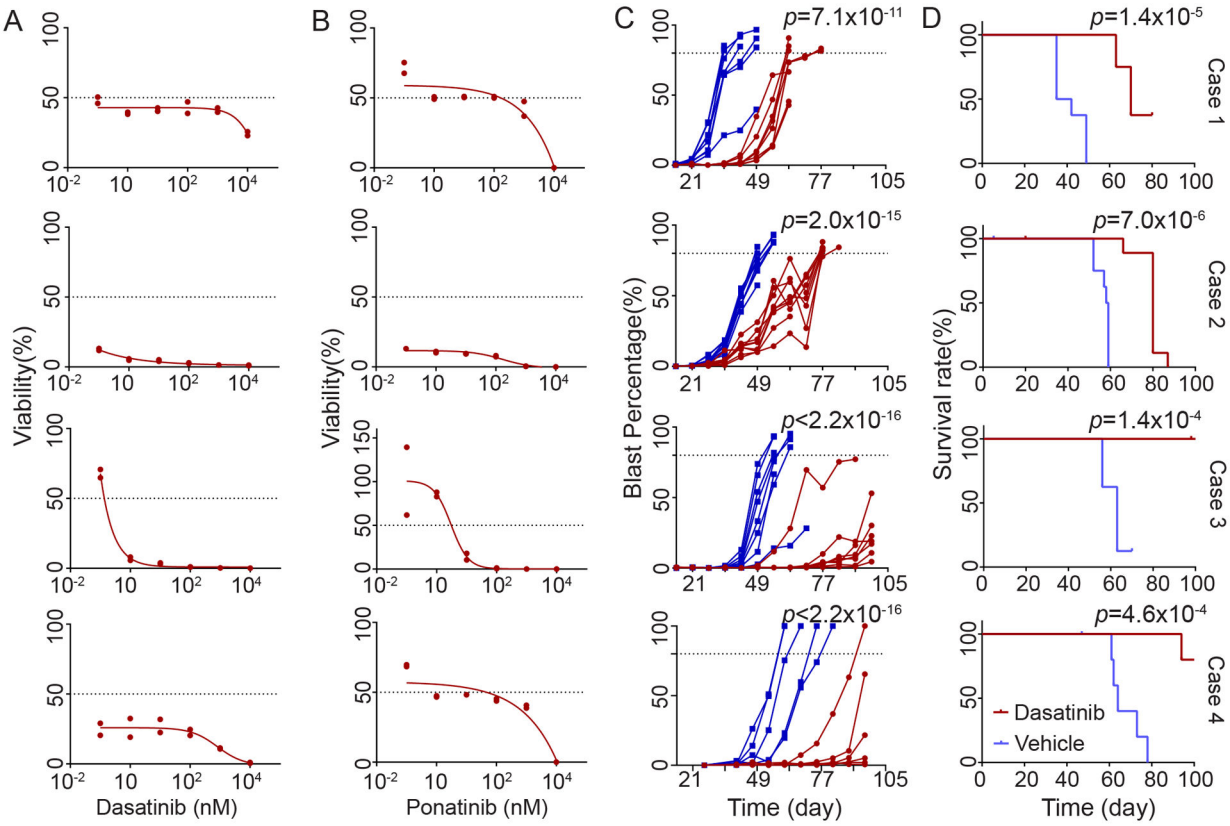

Figure 2. ***In vivo*** **efficacy of dasatinib therapy in T-ALL.**

A-B. Dose-response curves of dasatinib (A) and ponatinib (B) in T-ALL PDX cells used for *in vivo* efficacy studies. Leukemia cells were incubated with increasing concentration of drugs for 96 hours in the stromal cell co-culture system and cell viability was quantified using flow cytometry, as described in Methods. For each paitent sample at each drug concentration, cells were tested in duplicate. **C.** Leukemia burden in peripheral blood as a function of time in each T-ALL PDX models treated with dasatinib or vehicle. Dasatinib was given at 10mg/kg/day for 98 days until endpoint is met (e.g., leukemia burden reaches 80% or moribund for other reasons). *In vivo* efficacy of dasatinib treatment in PDX mouse model. P value was estimated using ANOVA test. Each curve represents an indidual mouse. **D** leukemia-free survival estimated for each T-ALL PDX model. The dasatinib treatment arm is shown in red curves and the vehicle treatment arm is shown in blue curves. P value was estimated using Cox regression model. Each treatment arm included 8 mice for cases 1, 2, and 3, and 6 mice per arm for case 4.

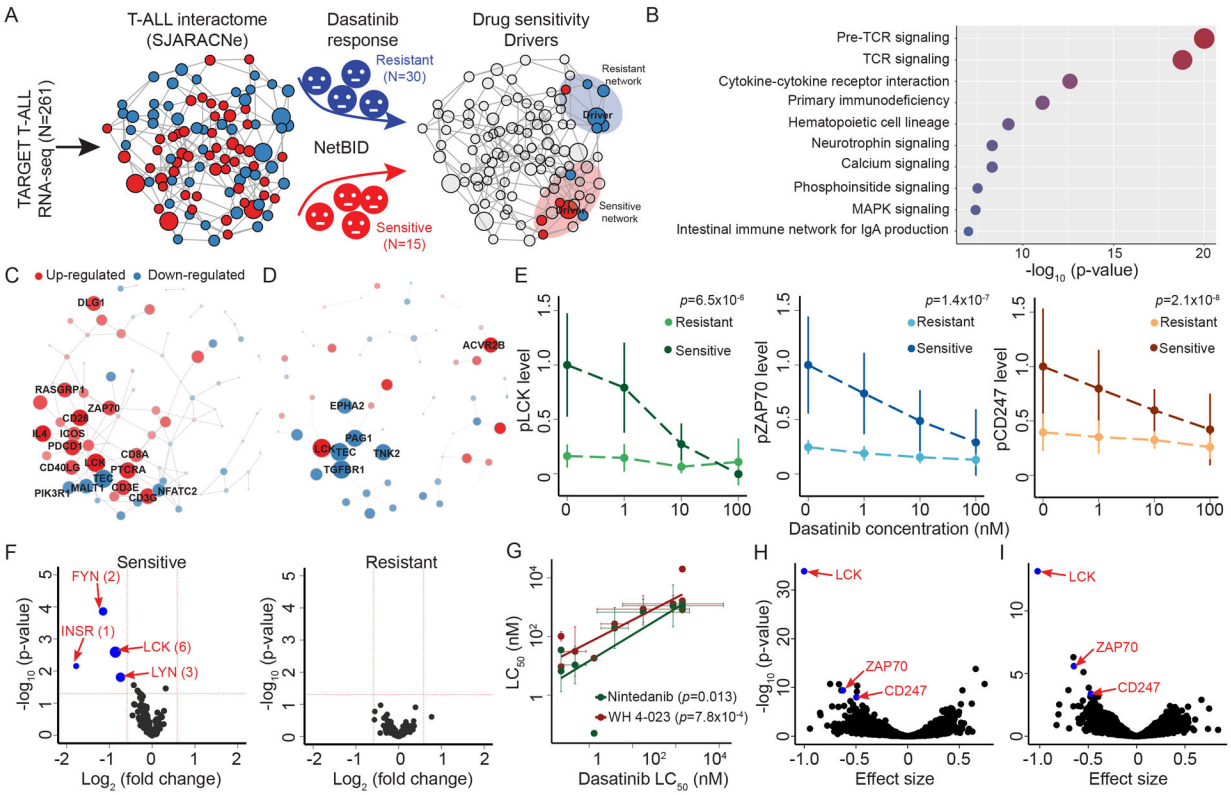

Figure 3. preTCR-LCK activation drives dasatinib sensitivity in T-ALL.

A Schema of the NetBID analysis for identifying drug sensitivity driver. By applying the SJARACNe algorithm to the published TARGET T-ALL RNA-seq dataset (N=261 patients), we first constructed a T-ALL interactome to describe signaling network in this leukemia. Then we perform network-based inference of gene activity (NetBID) using RNA-seq data of dasatinib-sensitive vs -resistant T-ALL (N=15 and 30 patients, respectively). Comparing gene activity between two groups, we identify drivers/master regulators of drug response. **B.** Pathway analysis of driver genes associated with dasatinib sensitivity. A total of 461 drug sensitivity driver genes were identified by using NetBID. Fisher exact test was used to assess the over-representation of each gene set in KEGG database in the drug sensitivity driver genes. **C-D.** Associations of preTCR pathway genes (C) and dasatinib target genes (D) with dasatinib sensitivity in T-ALL. Genes are shown as dots in networks based on their relationships defined by the T-ALL interactome, using SJARACNe. Driver genes up- and down-regulated in dasatinib-sensitive cases were marked as red and blue, respectively. Dot size corresponds to the P-value comparing gene activity in dasatinib-sensitive vs. -resistant cases. **E.** Phosphorylation level of LCK, ZAP70 and CD247 in fresh T-ALL PDX cells treated with various concentrations of dasatinib. Leukemia cells were incubated with dasatinib for 1 hour and phosphorylation was quantified by flow cytometry after intracellular staining with antibodies specific to each phospho-protein. Y-axis shows relative phospho-level of each molecule, with no drug as 100%; and x-axis indicates dasatinib concentration. Sensitive samples (N=7 independent PDX models) were plotted in dark colors while resistant samples (N=4 independent PDX models) were labeled in light colors. P value was estimated using Wilcoxon rank test. **F.** Phospho-proteomic profiling of dasatinib-sensitive vs

resistant T-ALL (N=3 and 2 independent T-ALL PDX cases, represented by the left and right panels, respectively). T-ALL PDX cells were treated with dasatinib (10 nM for 1 hour) and subjected to TMT-based phospho-proteomics. Kinase activity was estimated on the basis of phosphorylation of known substrates (see Methods) and compared between baseline and after-dasatinib treatment. In the Volcano plots, each dot represents a unique kinase and the degree to which its activity is affected by dasatinib is indicated by Log_2 transformed fold change (dasatinib treated versus baseline, x-axis) and–log_{10} transformed P-value (estimated using two-sided t test) (y-axis). Kinases with significant changes by dasatinib treatment are highlighted in blue and their sizes represent the number of known substrate phosphorylation sites. **G.** Correlation of dasatinib LC_{50} with that of LCK-specific inhibitors nintedanib and WH 4–023 (green and red, respectively) in T-ALL PDX cells (N=11 cases). P values were estimated using Pearson correlation test. **H-I.** Genome-scale CRISPR-Cas9 screening of T-ALL cell lines (N=3 unique cell lines) compared to all other cancer cell lines (N=686 cell lines) (H) or other hematologic malignancy cell lines (N=73 cell lines) (I). Each point represents one gene in the screen. The effect size on the x-axis represents the mean difference in dependency score between the T-ALL lines compared to other cell lines screened with negative effect size indicating greater dependency in T-ALL compared to other cell lines. The y-axis represents the statistical significance of enrichment calculated as -log_{10}(q-value) from a two-sided t-test with Benjamini Hochberg correction. Standard deviation is plotted as error bar.

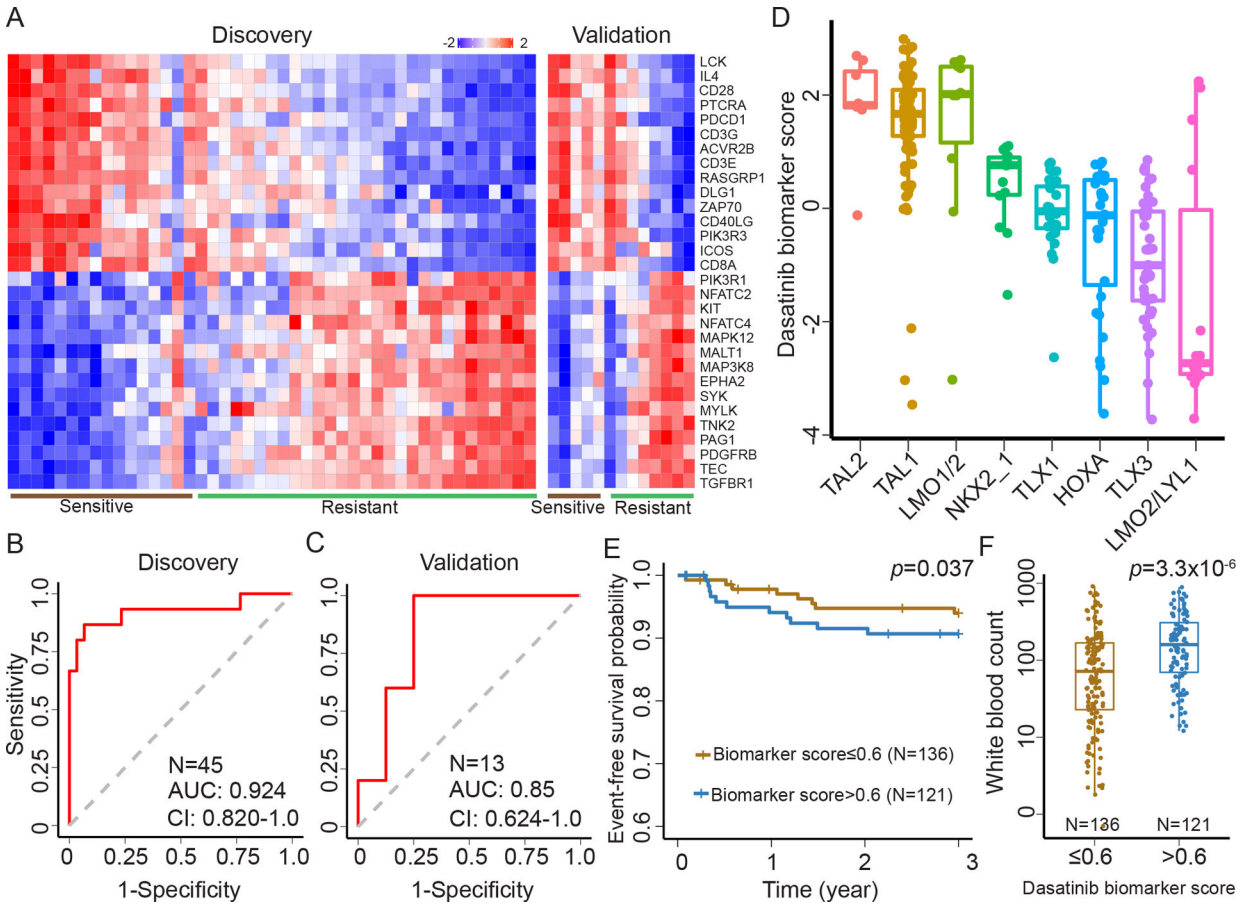

Figure 4. Biomarker model predicts dasatinib sensitivity across T-ALL subtypes.

A. Heatmap of NetBID-inferred activity of 30 drug sensitivity driver genes in the dasatinib pharmacotyping cohort as discovery (N=45 patients) and in the validation set (N=13 patients). To identify this panel, the 461 drivers associated with *ex vivo* dasatinib response were filtered against the preTCR pathway genes and known dasatinib targets. The top 15 rows show genes associated with dasatinib sensitivity while the bottom 15 rows represent genes driving dasatinib resistance. **B-C.** receiver operating characteristic curve analysis of the dasatinib biomarker score performance in the discovery and validation cohorts, respectively. **D.** Predicted dasatinib sensitivity in the TARGET T-ALL cohort (N=261) using the biomarker model. A biomarker score was estimated for each T-ALL case from its RNA-seq data and NetBID-inferred gene activity. T-ALL subtypes were defined as previously described[8] (Liu *et al.*, 2017). **E.** Survival analysis of T-ALL cases predicted as dasatinib-sensitive vs -resistant in the TARGET cohort (dasatinib biomarker score > or ≤ 0.6), indicating disparate treatment outcome of conventional chemotherapy. P value was estimated using Cox regression with the biomarker score as a continuous variable. **F.** White blood cell count at diagnosis was compared between T-ALL cases with predicted dasatinib sensitivity vs resistance in the TARGET cohort. P value was estimated using Wilcoxon rank test. Boxplots show summary of data in terms of the minimum, maximum, sample median, and the first and third quartiles.

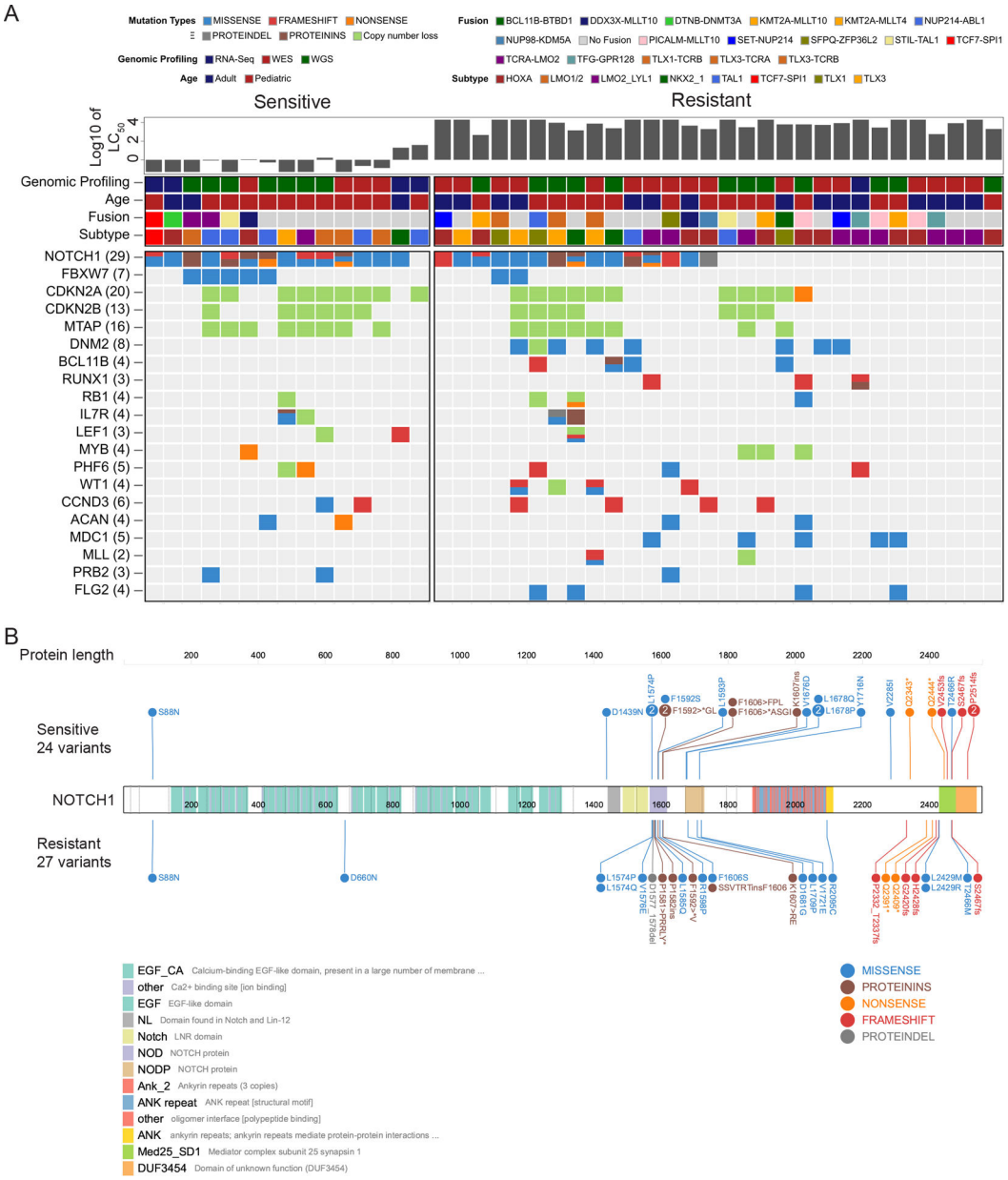

Figure 5. Somatic genomic abnormalities in dasatinib-sensitive T-ALL.

A. Oncoplot summarizes somatic genomic abnormalities in the T-ALL pharmacotyping cohort. Each column represents one sample and its dasatinib sensitivity is listed in the top row. Cases with *SPI1*-rearrangement are marked as red in the "Fusion" row. The type of genomic profiling (whole exome seq and/or RNA-seq) is indicated in the second row. Genomic data analyses (fusion gene and sequence mutation calling) were performed as described in Methods. **B.** *NOTCH1* mutations were more common in dasatinib-sensitive T-ALL compared to cases resistant to this drug (shown in the top and bottom panel, respectively). Mutation calling was performed using pipeline described previously and in Methods, from paired whole exome-seq, whole genome-seq, and/or leukemia RNA-seq.

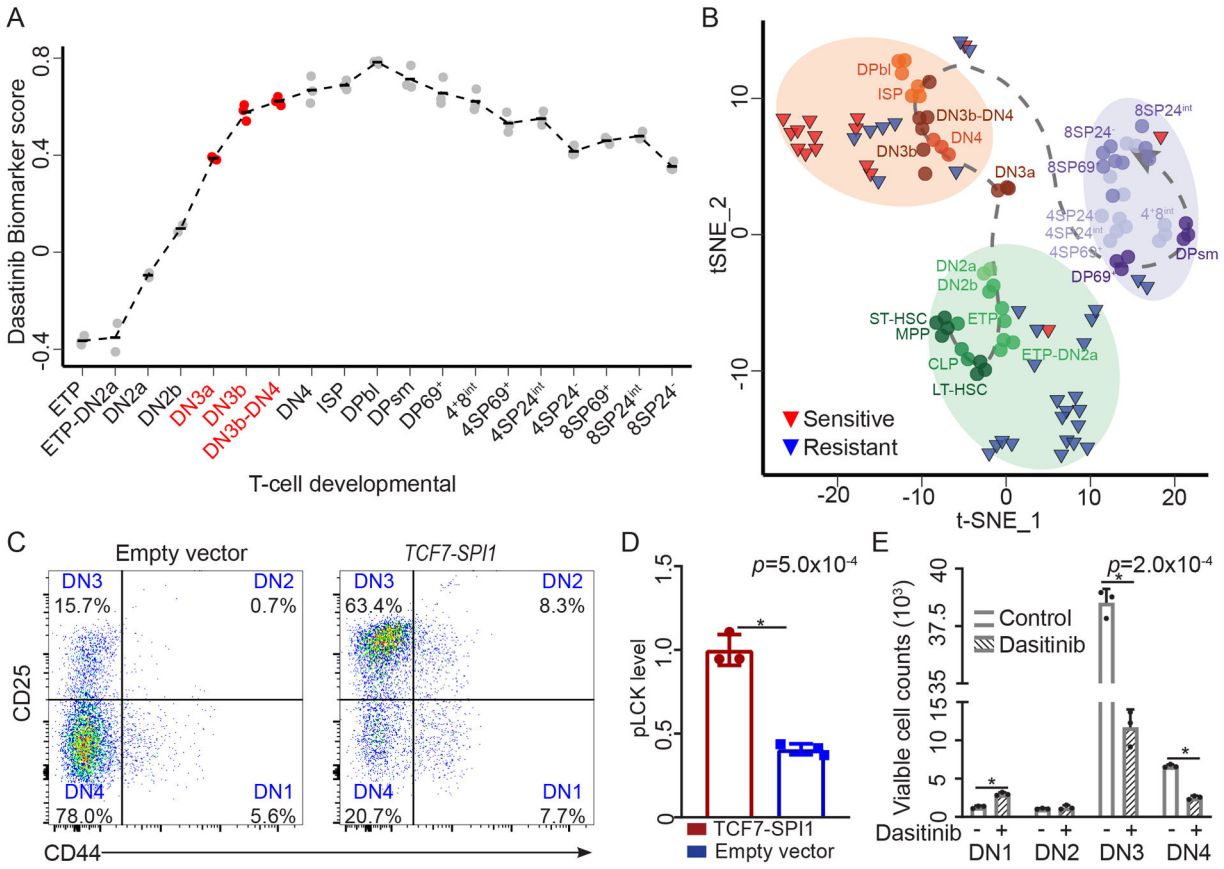

Figure 6. Association of T cell differentiation arrest with dasatinib sensitivity in T-ALL.

A. Inferred dasatinib sensitivity biomarker score for 19 mouse T-cell populations representing different developmental stages (N=3 mice for each stage). Published RNA expression profile[50] (Mingueneau *et al.*, 2013) was used as input of NetBID to infer gene activities from which dasatinib biomarker score was calculated. Dasatinib biomarker score approached the maximal level starting at DN3a-DN3b-DN4 stage (highlighted in red). Horizontal bars indicate the mean biomarker score for each T cell population. **B.** Differentiation stage of dasatinib-sensitive vs -resistant T-ALL. NetBID-based gene activity profiles of human T-ALL and mouse T cells from differentiation stages[50] (Mingueneau et al., 2013) were pooled after mapping to the same set of genes using BioMart. 465 genes had a coefficient of variation >0.5 and were included in clustering analysis using tSNE. Shaded circles represent three distinctive clusters inferred using the *k*-means method. Circle and triangle indicate T-ALL and normal T cell populations, respectively . **C.** Developmental arrest at DN3 stage of mouse hematopoietic stem and progenitor cells by ectopic expression of *TCF7-SPI1*. Mouse Lin-Sca+Ckit+ (LSK) cells were isolated from bone marrow and transduced lentivirally with SPI1 fusion gene or empty vector, followed by *in vitro* differentiation in the presence of OP9-DL1 cells, with Il7 and Flt3 ligand. The upper panels show CD25 and CD44 expression pattern in CD4/CD8 double negative population by flow cytometry, to define DN1, 2, 3, and 4 populations as labeled. **D.** LCK phosphorylation in mouse LSK cells transduced with *TCF7-SPI1* expression vector and empty vector. At the end of *in vitro* differentiation assay (Panel C), mouse cells were subjected to pohopho-flow

cytometry using LCK (Y394) antibody. Standard deviation was estimated from N=3 independent transduction and P value was derived from two-sided t test. **E.** Growth inhibition of mouse DN3 thymocytes by dasatinib *in vitro.* Primary mouse CD4 and CD8 double-negative thymocytes were isolated from thymus and incubated with dasatinib (100nM) for two days. Viable cell counts were performed by flow-cytometry using DAPI. DN3 T cells show the highest sensitivity to dasatinib. *P<0.05, P values for DN1, 2, 3 and 4 are 0.000388, 0.395572, 0.000043 and 0.000020, respectively. P values were estimated by two-sided t test. Standard deviation is plotted as error bar and is derived from N=3 unique mice. Center value represents mean.

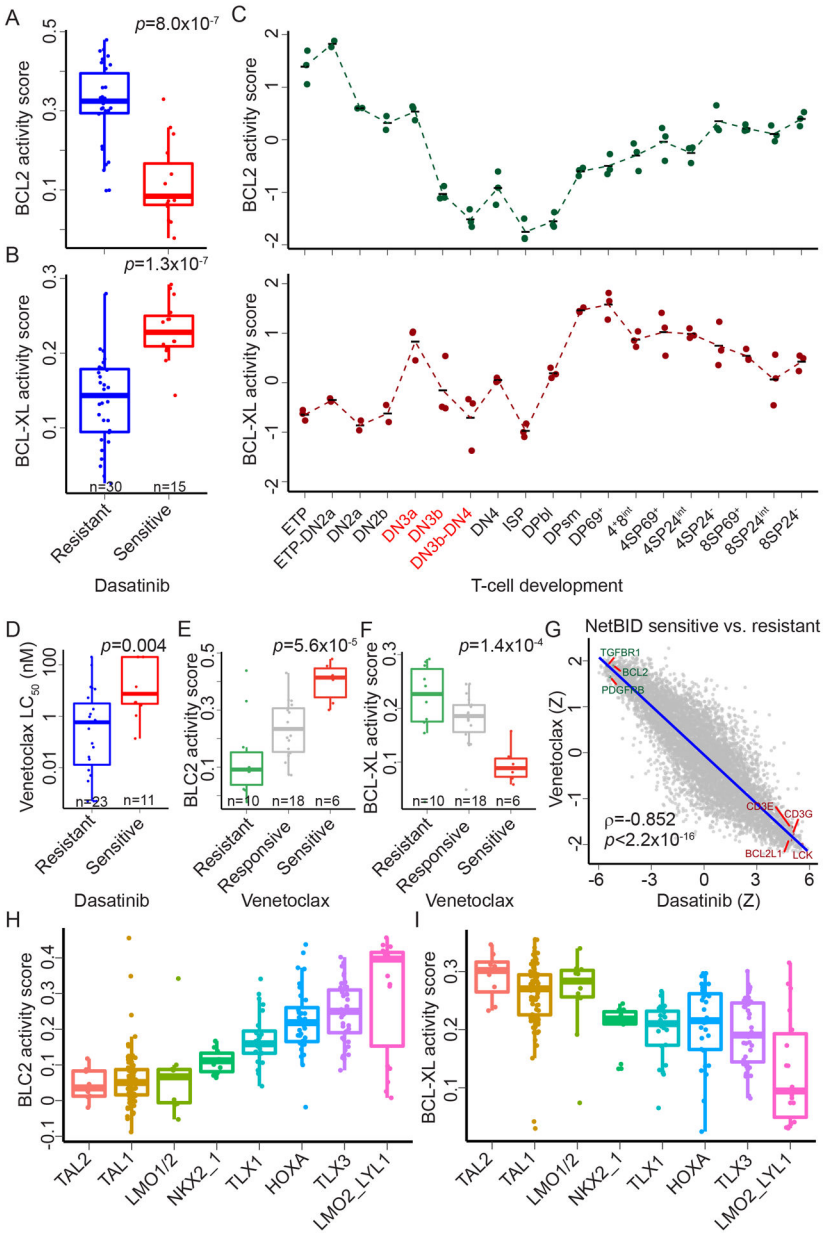

Figure 7. Differentiation-dependent activation of BCL2 and BCL-XL and its relation to T-ALL response to dasatinib and venetoclax A-B.

Association of BCL2 (**A**) or BCL-XL (**B**) activity with dasatinib sensitivity in T-ALL. Gene activity was inferred by NetBID analyses of the N=45 cases in the T-ALL pharmacotyping cohort and compared between dasatinib-sensitive and -resistant samples with P values estimated using two-sided t-test. **C.** Dynamic change of BCL2 and BCL-XL activity across normal T-cell differentiation stages (N=3 for each stage and bar represents the mean for each population). Gene activity was estimated from published mouse gene expression dataset[50] (Mingueneau *et al.,* 2013), as described in Figure 6. DN3a/DN3b/DN3b-4 stages are highlighted in red. **D.** Dasatinib sensitivity was associated with venetoclax resistance in T-ALL. Within N=45 cases in the T-ALL pharmacotyping cohort, N=34 were tested for venetoclax sensitivity *ex vivo*, Venetoclax LC_{50} was compared between dasatinib-sensitive

vs -resistant T-ALL, with P values estimated using two-sided t-test. In the same cohort, T-ALL sensitivity to venetoclax was associated with high BCL2 and low BCL-XL activity, respective (**E** and **F,** N=10, 18, 6 patients in the Resistant, Responsive, and Senstive groups, respectively). P values were estimated using ANOVA. **G.** Inverse correlation of the effects of gene activity on dasatinib sensitivity vs venetoclax sensitivity in T-ALL. Each dot represents a gene with Z-score plotted on the x and y axis to indicate the association of its activity with dasatinib and venetoclax sensitivity, respectively, as estimated by NetBID in the T-ALL pharmacotyping cohort. Marked in red are example genes up-regulated in dasatinib-sensitive cases but downregulated in venetoclax-sensitive cases. Those marked in green exhibited the opposite pattern of association with drug sensitivity. Correlation of two sets of Z scores was evaluated using Spearman correlation test. **H-I.** BCL2 and BCL-XL activity across subtypes in TARGET cohort (N=261 patients). Boxplots show summary of data in terms of the minimum, maximum, sample median, and the first and third quartiles.

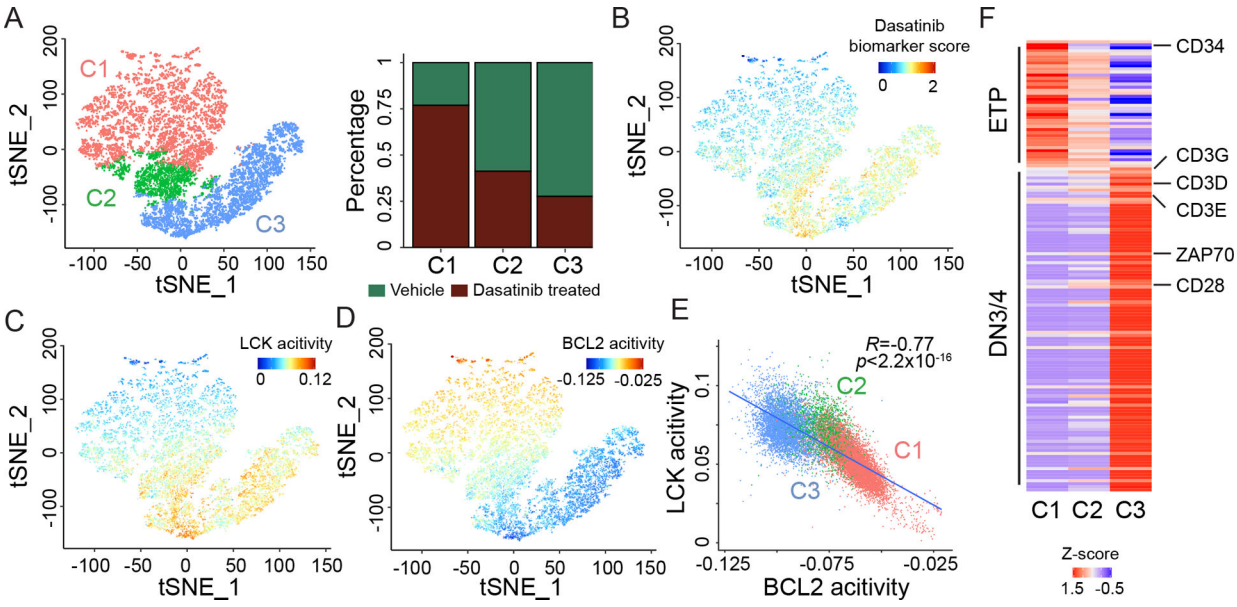

Figure 8. Single cell transcriptomic analysis identified intra-leukemia heterogeneity in LCK and BCL2 signaling, T-cell maturation, and dasatinib response.

T-ALL cells from SJ65 were incubated with dasatinib or vehicle for 4 days *in vitro*. scRNA-seq was then perfomred using viable cells from each group separately but transcription profiling data was pooled for subsequent analyses. Vehicle-treated cells mimiced naïve and sensitive to dasatnib whereas cells survived dasatinib exposure (dasatinib-treated) represented drug resistant cell population. **A.** Left panel, unsupervised clustering analysis of scRNA-seq of vehicle and dasatinib-treated T-ALL cells from SJ65. Each dot represent a single cell visualized in a two-dimensional projection by t-SNE. Three clusters (C1, C2, and C3, in red, green, and blue, respectively) were identified using k-means clustering. Right panel, cell composition of each cluster is visualized by stack plot with red and green indicating the % of cells from vehicle or dasatinib-treated samples. C1, C2, and C3 consisted of increasing proportion of naïve dasatinib-sensitive cells, representing populations with low, intermediate, and high sensitivity to dasatinit, respectively. **B.** Distribution of dasatinib biomarker score across three clusters, with C3 showing the highest predicted sensitivity and greatest proportion of vehicle-treated cells. **C.** LCK activity was highest in cluster C3, intermediate in C2, and lowest in C1, paralelling the proportion of dasaitnib-sensitive population. LCK activity is color-coded (from low to high, blue–red) on t-SNE plot. **D** BCL2 activity was lowest in cluster C3, intermediate in C2, and highest in C1, paralelling the proportion of dasaitnib-sensitive population. BCL2 activity is color-coded (from low to high, blue–red) on t-SNE plot. **E.** Inverse correlation of LCK and BCL2 activity at the single cell level in SJ65. Each dot represent a cell and color discriminate clusters C1, C2, and C3 (red, green, and blue, respectively). Correlation coefficient and P value were estimated using Pearson correlation. **F.** Differentiation stage of each population was prejected by examining the gene expression signature charateristic of ETP or DN3/DN4 T cells. Signature was derived from differential expression analysis of mouse T cell expression dataset[50] (Mingueneau *et al.,* 2013). Heatmap indicates the average of each gene (rows) for cells within each cluster (columns), after Z-normalization.